1966

Cross-spectral density measurements in a coupled-core reactor

Richard Allan Hendrickson
Iowa State University

CROSS-SPECTRAL DENSITY MEASUREMENTS IN A COUPLED-CORE REACTOR

by

Richard Allan Hendrickson

A Dissertation Submitted to the
Graduate Faculty in Partial Fulfillment of
The Requirements for the Degree of
DOCTOR OF PHILOSOPHY

Major Subject: Nuclear Engineering

Approved:

Signature was redacted for privacy.
In Charge of Major Work

Signature was redacted for privacy.
Head of Major Department

Signature was redacted for privacy.
Dean of Graduate College

Iowa State University
Of Science and Technology
Ames, Iowa

1966

TABLE OF CONTENTS

I. INTRODUCTION

The acceptance of noise analysis as a useful tool in the investigation of the kinetic behavior of nuclear systems has been somewhat conservative. The basic question of the need of statistical description as it applies to the gross behavior of neutronic processes was founded on the observation that the high neutron population density and relatively long lifetime found in most reactor cores permit adequate characterization of reactor kinetic behavior through solutions of deterministic equations. However, it is now recognized that there are many experimental situations which dictate the use of the stochastic model as the only adequate method for describing reactor behavior (16).

It has been known for some time that it is possible to determine kinetic parameters from reactor noise measurements since the noise is characteristic of the nuclear system in which it occurs (9, 19). Nuclear systems permit statistical description because the processes of fission, absorption, leakage, etc., are discontinuous processes based on transformations produced by discrete quantities. An equilibrium between destructive and productive processes never exists on a microscopic time scale, but a time-averaged steady-state condition is possible.

Noise analysis techniques have been used to monitor the initial startup of new reactors by searching for potential

instabilities such as sharp resonances in the power spectrum (24). If a resonance becomes narrower with increasing power, an estimate of the threshold of stability may be determined. The shutdown margin of a subcritical system can be deduced from the shape of the noise spectrum if the neutron lifetime is known (1).

The presence of experimental apparatus, such as a reactivity oscillator, perturbs the characteristics of the core that is being investigated. The noise analysis method may be employed to avoid disturbing the measured quantity by observing small variations of the dependent variables during the normal operation of the reactor.

In the analytical treatment of a non-linear system, such as a nuclear reactor, a useful technique often employed to reduce the non-linear equations to linear form involves the use of an incremental model. During the experimental verification of an incremental model, the system must operate within the limits of linearity. Measurements based on reactor noise are subject to minimum non-linear distortion since the input signal amplitude is bounded by the inherent fluctuations of the dependent variable about a mean value.

Analyses of the power spectral density of the random variations of the neutron density induced by the inherent noise spectrum of the fission process have been performed at several laboratories with varying degrees of success (1,

9, 13, 14). These measurements were performed under adverse conditions due to the presence of extraneous noise sources which partially mask the desired component of the random signal. Crosscorrelation techniques, when properly applied, substantially reduce the extraneous noise problem and present a method of analyzing the joint properties of two random variables. In this study, a cross-spectral density technique was applied to the two-core UTR-10 reactor.

One method of analyzing the kinetic behavior of a reactor transforms the spatial configuration of the reactor into a set of points or nodes, where each node represents a selected part of the reactor volume. The descriptive equations reduce to a set of coupled, ordinary differential equations, with the dependent variables being the average neutron density in each region. Coupling coefficients, which represent the exchange of neutrons between regions, appear in the set of equations. The coupling coefficients may be obtained from detailed spatial calculations.

The objectives of this investigation were to develop the cross-spectral density method of obtaining the reactivity coupling coefficient of a coupled-core reactor and to describe the experimental techniques involved in estimating the ratio of the reactivity coupling coefficient to the mean generation time of the neutrons in the cores.

II. LITERATURE SURVEY

This section contains a brief survey of contributions to the field of reactor-noise analysis in general, models of coupled-core systems, and applications of random-noise theory to the study of coupled-core reactor kinetics.

Several disadvantages associated with oscillator tests performed in research and power reactors prompted the adoption of power spectral measurements soon after Moore (19) combined the theories of stochastic processes and reactor kinetics. He thereby obtained the famous result which relates the square modulus of the reactor transfer function to the Fourier transform of the autocorrelation function of the noise power of the reactor. Although the exact form of the input noise spectrum is unknown, many investigators have assumed the input spectrum to be white.

Using a tunable band-pass filter, Cohn (9) measured the mean square noise amplitude of several low-power experimental facilities at Argonne National Laboratory. He was able to determine the ratio of the effective delayed neutron fraction to the prompt neutron lifetime in fast reactors where high frequency measurements became exceedingly difficult when other techniques were employed.

Moore (20) then developed a formalism which may be used to calculate the noise transfer function corresponding to any given kinetic model. Fluctuation and noise correlation

matrices were defined. Cross-spectral density functions relating the macroscopic variables were derived from the Fourier transformed correlation matrices. It is possible, using Moore's formulation, to determine reactor parameters under conditions of no external excitation and retain the uncorrelated-noise rejection characteristics of cross-correlation techniques.

Cohn (10) proposed a noise-equivalent source obtained from the Schottky formula (which calculates the noise due to the random flow of electrons in a diode). The analogy to production, absorption, and leakage of neutrons holds because all of these processes obey the Poisson distribution. It was noted that the spectral density of the noise-equivalent source is independent of frequency, and thus the noise input is white.

The question of the unknown character of the noise-input spectrum was raised again by Griffin and Randall (13) when power spectral density measurements at SRE failed to agree at low frequencies (less than one cycle per second) with oscillator test data. The conclusion was that some unknown in-core phenomenon was altering the low frequency "whiteness" of the reactor-driving spectrum.

Balcomb, et al., (2) employed crosscorrelation techniques to measure the impulse response of Godiva and Kiwi-A3. This method required short operating times (especially

important for Kiwi) compared to the duration of sinusoidal oscillation experiments. To circumvent the unknown input spectrum problem, small amplitude, externally controlled perturbations, which preserved the system linearity, were used. Also, useful data were obtained in the presence of strong noise sources. The mean neutron lifetime of Kiwi-A3 was determined from the break frequency of the Fourier transformed impulse response data.

To overcome the limitations of instrument noise, always present in autocorrelation analyses, Rajagopal (22) independently undertook a problem similar to the work of Balcomb, et al. Crosscorrelation data were obtained from continuous multiplication of the input-output signals recorded on a moveable-head F.M. magnetic tape recorder. Input signals were derived from an electro-mechanical reactivity oscillator driven by signals obtained from a detector observing the random disintegration of a radioactive source. Different time lags were achieved by varying the length of the magnetic tape between the heads. A value of prompt neutron lifetime was determined from the transfer function amplitude. The spectral data of Balcomb, et al., and Rajagopal terminated at an upper limit of approximately 20 cycles per second.

One kinetic model employed in describing single-core reactor behavior has been the space-independent or point

reactor approximation. Investigation of the kinetic behavior of coupled-core reactors presents an additional complication over those systems cited above. The space-averaged parameters of a coupled system are subject to the influence of the spatial shape of the neutron flux. Danofsky and Uhrig (12) have shown that flux tilting in a two-core reactor affects the worth of the control rods. Henry and Curlee (15) suggested that the space-time-variable separability difficulties encountered in describing the transient response of a single core reactor could be alleviated by writing separate kinetic equations for fuel regions separated by pure scattering media. Each equation includes a thermal source term determined from a diffusion approximation of the neutron current at the fuel-scattering medium interface.

Baldwin (3) considered this approximation in relation to the Argonaut reactor. He derived the kinetic equations by including an interaction term within the source term of the thermal neutron diffusion equation. The interaction term is proportional to the flux in the opposite slab at an earlier time. The constant of proportionality is taken as a measure of the exchange or interaction reactivity between fuel regions.

Boynton and Uhrig (7) employed the random reactivity input device built by Rajagopal to excite one slab of the two-core UFTR which in turn drove the opposite core. Analysis of the cross-spectrum of the outputs of the two cores provided

a measurement of the multiplication factor of the individual cores. The phase angle of the cross-spectral density function was sensitive to the time required for a neutron disturbance to travel between cores. They concluded that the value of transit time should be determined from the velocity of a neutron wave. An expression was developed that required measurement of the power spectral density of the input (neutron density of the externally excited core) and the cross-spectral density of the input and output (neutron density of the opposite core). The power spectral measurements were plagued by extraneous noise interference so that only phase-angle information from the cross-spectral measurements was used.

Leribaux (18) extended the formalism of Moore by introducing additional noise sources and applying the results in a theoretical and experimental study of the kinetic behavior of the coupled-core UTR-10 reactor.

Crosscorrelation measurements were performed in the UTR-10 by Danofsky (11). Voltage fluctuations obtained from two sets of ion chambers and micromicroammeters were recorded on 35-mm movie film, manually sampled, and programmed for calculation of correlation and spectrum functions on a digital computer. A method of measuring the reactivity coupling between the cores of the reactor was developed.

III. THEORY

A. Fundamental Concepts

Explicit mathematical relationships can describe, with reasonable accuracy, many physical phenomena. However, many physical situations arise in which a deterministic approach is impractical. If a particular system produces data that are random in character, the phenomenon must be described in terms of probability conditions and statistical averages.

Data obtained from dynamic systems are normally characterized as being functions of time and for purposes of this study will be described in this manner. A single time history representing a random phenomenon is called a sample function, and if observed during a finite time interval it is termed a sample record (5). The collection (the ensemble) of all possible sample functions is called a random or stochastic function.

The first moment, or mean value, of the random function $\{x(t)\}$ (the brackets signify an ensemble of sample functions) is calculated from the expression

$$\overline{x(t_1)} = \lim_{N\to\infty} \frac{1}{N} \sum_{k=1}^{N} x_k(t_1) \tag{1}$$

and the joint moment is given by

$$\varphi_{xx}(t_1, t_1 + \tau) = \lim_{N\to\infty} \frac{1}{N} \sum_{k=1}^{N} x_k(t_1) x_k(t_1 + \tau) \tag{2}$$

The joint moment in this case is a correlation between the values of the random function at two different times and is called an autocorrelation function. If $\overline{x(t_1)}$ and $\varphi_{xx}(t_1, t_1 + \tau)$ do not vary as time t_1 varies, the random process is defined as stationary. In the practical sense, the stationary property allows the calculation of statistical properties using an arbitrary time origin.

If the random function $\{x(t)\}$ is stationary, and $\overline{x(k,t)}$ and $\varphi_{xx}(\tau,k)$, for the k^{th} sample function, given by

$$\overline{x(k,t)} = \lim_{T\to\infty} \frac{1}{T} \int_0^T x_k(t)dt \tag{3}$$

and

$$\varphi_{xx}(\tau,k) = \lim_{T\to\infty} \frac{1}{T} \int_0^T x_k(t)x_k(t+\tau)dt \ , \tag{4}$$

do not differ when computed over different sample functions, the random function is ergodic. The ergodic property permits the calculation of time-averaged properties from a single sample function. That is,

$$\overline{x(k,t)} = \overline{x(t)}$$

and

$$\varphi_{xx}(k,\tau) = \varphi_{xx}(\tau) \ .$$

It is common practice to assume that random data representing

stationary physical phenomena are ergodic. Therefore the ergodic property is assumed to hold for all random functions involved in this investigation. A random ergodic function is necessarily stationary.

B. Autocorrelation and Power Spectral Density Functions

The autocorrelation function describes the dependence of the values of a function at one time to the values of the same function taken at another time. The autocorrelation function of the random variable x(t) is

$$\varphi_{xx}(\tau) = \lim_{T\to\infty} \frac{1}{2T} \int_{-T}^{T} x(t)x(t+\tau)dt \ . \qquad (5)$$

φ_{xx} is an even function of the time displacement τ, with a maximum at $\tau = 0$. The mean value of x(t) is given by

$$\overline{x(t)} = [\varphi_{xx}(\tau\to\infty)]^{1/2}$$

that is, if the function x(t) has a non-zero mean, the autocorrelation function converges to the square of the mean value of x(t) as τ becomes very large. Generality is not lost if $\overline{x(t)}$ is assumed to be zero. It is necessary only to realize that x(t) is measured as a fluctuation about its mean value. It is clear that when the displacement τ is zero, the autocorrelation function equals the mean square

value of x(t).

The function

$$x_T(t) = \begin{cases} x(t) & -T \leq t \leq T \\ 0 & t > |T| \end{cases}$$

is introduced, and the power spectral density Φ_{xx} is defined as

$$\Phi_{xx}(\omega) = \lim_{T \to \infty} \frac{1}{2T} |X_T(\omega)|^2 , \tag{6}$$

where

$$X_T(\omega) = \int_{-\infty}^{\infty} x_T(t) e^{-j\omega t} dt . \tag{7}$$

Under appropriate mathematical conditions (4, 17), the autocorrelation function and the power spectral density are related by the Fourier transform, thus,

$$\varphi_{xx}(\tau) = \frac{1}{2\pi} \int_{-\infty}^{\infty} \Phi_{xx}(\omega) e^{j\omega\tau} d\omega \tag{8}$$

$$\Phi_{xx}(\omega) = \int_{-\infty}^{\infty} \varphi_{xx}(\tau) e^{-j\omega\tau} d\tau . \tag{9}$$

Φ_{xx} is a real, positive, and even function of the angular frequency. Mathematical convenience dictates using values of negative frequency, but only positive frequencies exist in a physical situation.

Two main difficulties arise when power spectrum measure-

ments are employed. Extraneous noise present in the system reduces the accuracy of measurements. Second, the real-valued character of the power spectral density deprives the investigator of phase angle information.

C. Crosscorrelation and Cross-spectral Density Functions

In many physical problems it is desirable to investigate common properties of two random functions. The ergodic property is again assumed in defining the crosscorrelation function between the random variables x(t) and y(t) as

$$\varphi_{xy}(\tau) = \lim_{T\to\infty} \frac{1}{2T} \int_{-T}^{T} x(t)y(t+\tau)dt \tag{10}$$

$\varphi_{xy}(\tau)$ is not an even function, and it does not necessarily achieve a maximum at $\tau = 0$. The two random functions x(t) and y(t) are uncorrelated if their crosscorrelation function is identically zero.

The crosscorrelation function and cross-spectral density function form a Fourier transform pair (4, 17),

$$\varphi_{xy}(\tau) = \frac{1}{2\pi} \int_{-\infty}^{\infty} \Phi_{xy}(\omega)e^{j\omega\tau}d\omega \tag{11}$$

$$\Phi_{xy}(\omega) = \int_{-\infty}^{\infty} \varphi_{xy}(\tau)e^{-j\omega\tau}d\tau \ , \tag{12}$$

where the cross-spectral density function is defined by

$$\Phi_{xy}(\omega) = \lim_{T\to\infty} \frac{1}{2T} X_T^*(\omega) Y_T(\omega)$$

and the asterisk denotes the complex conjugate. $\Phi_{xy}(\omega)$ is generally a complex number, and it may be written as

$$\Phi_{xy}(\omega) = C_{xy}(\omega) - jQ_{xy}(\omega) \tag{13}$$

where the real part, $C_{xy}(\omega)$ is the co-spectral density function and the imaginary part, $Q_{xy}(\omega)$ is the quadrature spectral density function (5). The complex nature of the cross-spectrum permits the determination of phase-angle information between the input and output of a particular system. The determination of time delays through a system at a frequency ω is also possible. Another fundamental property of cross-spectrum measurements is the ability to reduce undesired noise information.

D. Matrix Formulation of the Cross-spectral Density

A formalism, published by Moore in 1959, that leads to an expression for the cross-spectral density between any two observable variables in a linear system will be described. It was Moore's intention to develop a means of calculating the (noise) transfer function corresponding to any given kinetic model of a reactor.

A general set of coupled equations which provides for

noise sources in any or all members of the set is the following:

$$Z_{11}x_1 + Z_{12}x_2 + \ldots + Z_{1n}x_n = f_1(t)$$

$$Z_{21}x_1 + Z_{22}x_2 + \ldots + Z_{2n}x_n = f_2(t)$$

$$\vdots$$

$$Z_{n1}x_1 + Z_{n2}x_2 + \ldots + Z_{nn}x_n = f_n(t) \qquad (14)$$

where

$$Z_{ij},\ (i,j = 1,2,\ldots,n)\ ,$$

are linear combinations of differential operators (of any order with respect to time) with constant coefficients;

$$x_j(t),\ (j = 1,2,\ldots,n)\ ,$$

is the j^{th} macroscopic dependent variable;

$$f_i(t),\ (i = 1,2,\ldots,n)\ ,$$

is the noise input function in the i^{th} loop. The variables $x_j(t)$ and $f_i(t)$ are assumed to be ergodic random functions.

Two matrices are now defined whose elements are given by the fluctuation (output) correlation function,

$$\varphi_{ij}(\tau) = \lim_{T\to\infty} \frac{1}{2T} \int_{-T}^{T} x_i(t)x_j(t + \tau)dt\ ,$$

$$i,j = 1,2, \ldots,n. \quad , \tag{15}$$

and the noise (input) correlation function,

$$\lambda_{lm}(\tau) = \lim_{T\to\infty} \frac{1}{2T} \int_{-T}^{T} f_l(t) f_m(t + \tau) dt \quad ,$$

$$l,m = 1,2, \ldots,n. \tag{16}$$

The fluctuation correlation matrix φ has elements φ_{ij}, and the noise correlation matrix λ has elements λ_{lm}.

It is convenient to introduce a fluctuation spectral density matrix Φ, according to the definition of the cross-spectral density function in Equation 12, whose elements are

$$\Phi_{ij}(\omega) = \int_{-\infty}^{\infty} \varphi_{ij}(\tau) e^{-j\omega\tau} d\tau \quad ,$$

$$i,j = 1,2, \ldots,n. \quad , \tag{17}$$

and a noise spectral density matrix Λ, whose elements are

$$\Lambda_{lm}(\omega) = \int_{-\infty}^{\infty} \lambda_{lm}(\tau) e^{-j\omega\tau} d\tau \quad ,$$

$$l,m = 1,2, \ldots,n. \tag{18}$$

In order to apply Equations 17 and 18, the condition of square integrability is satisfied when the correlation functions, φ_{ij} and λ_{lm}, tend to zero for large τ, which is essentially saying that the fluctuations must be measured from average values.

A connection must now be established between the φ_{ij} and λ_{lm}. A differential operator is chosen from the p^{th} loop of Equation 14, designated Z_{pj}, and modified so that differentiation is performed with respect to τ instead of t. This new operator is $\bar{Z}_{pj}$. Equation 15 is operated on with $\bar{Z}_{pj}$, thus,

$$\bar{Z}_{pj}\varphi_{ij}(\tau) = \lim_{T\to\infty} \frac{1}{2T} \int_{-T}^{T} x_i(t)\bar{Z}_{pj}x_j(t + \tau)dt \ . \qquad (19)$$

A summation on the j index gives

$$\sum_{j=1}^{n} \bar{Z}_{pj}\varphi_{ij}(\tau) = \lim_{T\to\infty} \frac{1}{2T} \int_{-T}^{T} x_i(t) \sum_{j=1}^{n} \bar{Z}_{pj}x_j(t + \tau)dt \ . \qquad (20)$$

Since t and τ are independent variables, the derivatives with respect to τ in $\bar{Z}_{pj}$ on the right side of Equation 20 can be replaced by derivatives with respect to $(t + \tau)$. The sum is then recognized to be the same as the left side of Equation 14 (p^{th} loop) with t replaced by $(t + \tau)$, i.e.,

$$\sum_{j=1}^{n} \bar{Z}_{pj}x_j(t + \tau) = f_p(t + \tau) \ . \qquad (21)$$

Equation 20 may now be written as

$$\sum_{j=1}^{n} \bar{Z}_{pj}\varphi_{ij}(\tau) = \lim_{T\to\infty} \frac{1}{2T} \int_{-T}^{T} x_i(t)f_p(t + \tau)dt. \qquad (22)$$

It follows that

$$\sum_{j=1}^{n} \bar{Z}_{pj}\varphi_{ij}(\tau) = \lim_{T\to\infty} \frac{1}{2T} \int_{-T+\tau}^{T+\tau} f_p(\alpha)x_i(\alpha - \tau)d\alpha \ , \quad (23)$$

when the change of variables $\alpha = t + \tau$ is introduced. Finally,

$$\sum_{j=1}^{n} \bar{Z}_{pj}\varphi_{ij}(\tau) = \lim_{T\to\infty} \frac{1}{2T} \int_{-T}^{T} f_p(t)x_i(t - \tau)dt \quad (24)$$

results when the ergodic property is applied.

Another operator is chosen from Equation 14 and modified so that (1) differentiation is performed with respect to τ instead of t, and (2) the derivatives of odd order in $\bar{Z}_{ij}$ have their signs changed. This operator, chosen from the q^{th} loop, is symbolized by $\bar{Z}^{+}_{qi}$. Equation 24 is operated on with $\bar{Z}^{+}_{qi}$ and gives, after summation on the i index,

$$\sum_{i=1}^{n}\sum_{j=1}^{n} \bar{Z}^{+}_{qi}\bar{Z}_{pj}\varphi_{ij}(\tau) = \lim_{T\to\infty} \frac{1}{2T} \int_{-T}^{T} f_p(t) \sum_{i=1}^{n} \bar{Z}^{+}_{qi}x_i(t - \tau)dt \ . \quad (25)$$

Derivatives with respect to τ can be replaced by derivatives with respect to $(t - \tau)$, but the odd order derivatives now have the opposite sign so that

$$\sum_{i=1}^{n} \bar{Z}^{+}_{qi}x_i(t - \tau) = f_q(t - \tau) \ . \quad (26)$$

With the substitution of Equation 26, Equation 25 becomes

$$\sum_{i=1}^{n}\sum_{j=1}^{n}\bar{Z}^{+}_{qi}\bar{Z}_{pj}\varphi_{ij}(\tau) = \lim_{T\to\infty}\frac{1}{2T}\int_{-T}^{T} f_p(t)f_q(t+\tau)dt$$

$$= \lim_{T\to\infty}\frac{1}{2T}\int_{-T-\tau}^{T-\tau} f_q(\gamma)f_p(\gamma+\tau)d\gamma$$

$$= \lim_{T\to\infty}\frac{1}{2T}\int_{-T}^{T} f_q(t)f_p(t+\tau)dt$$

$$= \lambda_{qp}(\tau) \qquad (27)$$

The relationship between the φ_{ij} and λ_{lm} is established through the system,

$$\sum_{i=1}^{n}\sum_{j=1}^{n}\bar{Z}^{+}_{qi}\bar{Z}_{pj}\varphi_{ij} = \lambda_{qp}(\tau)\ ,$$

$$q,p = 1,2,\ldots,n.\ , \qquad (28)$$

which represents n^2 linear differential equations in the $\varphi_{ij}(\tau)$. A Fourier transformation converts the n^2 coupled differential equations of Equation 28 to a set of n^2 simultaneous algebraic equations. Hence, with the aid of Equations 17 and 18,

$$\sum_{i=1}^{n}\sum_{j=1}^{n}\underline{Z}^{*}_{qi}\underline{Z}_{pj}\Phi_{ij}(\omega) = \Lambda_{qp}(\omega)\ , \qquad (29)$$

where

$\underline{Z}^{*}_{qi}$ is the complex conjugate of $\underline{Z}_{qi}$ obtained from

$\overline{Z}^{+}_{qi}$ by replacing the derivative operator $\frac{d}{d\tau}$ with $j\omega$;

$\underline{Z}_{pj}$ is obtained from $\overline{Z}_{pj}$ by replacing $\frac{d}{d\tau}$ with $j\omega$;

$\Phi_{ij}(\omega)$ and

$\Lambda_{qp}(\omega)$ are the output and input cross-spectral density functions, respectively.

The square integrability condition permits the φ_{ij} and λ_{lm} and their derivatives to vanish as $\tau \to \pm\infty$. In matrix form, Equation 29 becomes

$$\underline{Z}^{*}\Phi\underline{Z}^{T} = \Lambda \tag{30}$$

where $\underline{Z}^{T}$ is the transpose matrix of $\underline{Z}$, that is, $\underline{Z}_{pj} = \underline{Z}^{T}_{jp}$. If the matrix $\underline{Z}$ is non-singular, the matrix expression for the Φ_{ij} as a function of the Λ_{qp} is given by

$$\Phi = (\underline{Z}^{*})^{-1}\,\Lambda\,(\underline{Z}^{T})^{-1}\ , \tag{31}$$

or alternatively,

$$\Phi_{hk}(\omega) = \sum_{i=1}^{n}\sum_{j=1}^{n}(\underline{Z}^{-1})^{*}_{hi}\Lambda_{ij}(\omega)(\underline{Z}^{T})^{-1}_{jk}\ . \tag{32}$$

Equation 32 takes the more convenient form,

$$\Phi_{hk}(\omega) = \sum_{i=1}^{n}\sum_{j=1}^{n}(\underline{Z}^{-1})^{*}_{hi}\underline{Z}^{-1}_{kj}\Lambda_{ij}(\omega)\ , \tag{33}$$

when the following substitutions are performed:

$$(\underline{Z}^{*})^{-1}_{hi} = (\underline{Z}^{-1})^{*}_{hi}$$

$$(\underline{Z}^{T})^{-1}_{jk} = \underline{Z}^{-1}_{kj}$$

where

$$\underline{Z}^{-1}_{kj} = \frac{\text{Cofactor } (j,k) \text{ of } \underline{Z}}{\text{Determinant of } \underline{Z}} \quad . \tag{34}$$

It is possible to determine the cross-spectral density functions (and power spectral density functions when h = k) of the observable variables in a linear system from Equation 33. This matrix formulation also may be applied to the most complicated networks of input noise functions.

E. Kinetics Equations of a Coupled-core Reactor

The UTR-10 is a thermal, heterogeneous, light-water moderated and cooled reactor. The unusual feature of its design is that the fuel material is contained in two distinct regions (herein referred to as "cores") separated by 18 inches of graphite. Additional graphite surrounding these regions acts as a reflector. Each core behaves as a semi-independent, subcritical system with the exchange of (mostly) thermal neutrons between cores acting to sustain the critical operation of the reactor as a total system (3).

In spite of the relative mathematical simplicity of many

models formulated to describe the kinetic behavior of nuclear reactors, the successful application of these models to complicated reactor systems justifies their continued use. It is recognized that limitations exist because of the lack of detailed spatial description of the neutron flux, but somewhat surprisingly, the kinetic behavior predicted by space-averaged-variable and lumped-parameter models has been consistent with experimental measurements (1, 3, 7, 8, 11, 12, 14, 18, 22).

Two models are proposed that lead to cross-spectral density functions of the fluctuating neutron density in the two cores and in two experimental access locations adjacent to the two cores. The effects of delayed neutrons are neglected since the lower limit of frequency investigated (10 cycles per second) is much greater than the reciprocal time constant associated with the shortest-lived delayed neutron precursor. In both models, each core is assumed to be a separate, slightly subcritical, space-averaged, thermal reactor.

1. First Model

The kinetic equation for the i^{th} region is

$$\frac{dn_i(t)}{dt} = \frac{\delta k_i}{L_i} n_i(t) + \frac{\alpha_i}{L_i} n_j(t - \delta_{ij}), \quad (i \neq j = 1,2.) , \qquad (35)$$

where

$n_i(t)$ is the neutron density in the i^{th} core,

δk_i is the reactivity,

L_i is the generation time in the core (in the reciprocal production rate sense),

α_i is the reactivity coupling coefficient,

$n_j(t - \delta_{ij})$ is the neutron density at an earlier time in the j^{th} region, and

δ_{ij} is the time required for a disturbance to travel between cores.

The equation for region two is identical to that of region one except that the subscripts are interchanged.

The delay time, δ, is assumed to be a frequency dependent parameter that is best approximated by the time required for a neutron wave to traverse a given distance in a scattering medium (7, 11).

It is necessary to express the kinetic equations in a form that allows the application of the theory of random processes. Such a form would be one in which the fluctuations of $n_1(t)$ and $n_2(t)$ about their average values are related to the "driving" fluctuations of parameters such as fission, leakage, absorption, and exchange processes. The dependent or observable variables may be expressed as

$$n_i(t) = n_{io} + N_i(t), \; i = 1,2. \; , \tag{36}$$

where n_{io} is a steady-state or average term and $N_i(t)$ is the

time dependent fluctuation. The ratios $\delta k_i/L_i$ and α_i/L_i assume the following similar forms:

$$\frac{\delta k_i}{L_i} = r_{io} + R_i(t) \tag{37}$$

$$\frac{\alpha_i}{L_i} = a_{io} + A_i(t) \tag{38}$$

When Equations 36, 37, and 38 are substituted in Equation 35, products of fluctuating terms neglected, and steady-state relations eliminated, the resulting expression is

$$DN_i(t) = r_{io}N_i(t) + n_{io}R_i(t) + A_i(t)n_{jo} + a_{io}\sum_{m=o}^{\infty} \frac{(-\delta_{ij})^m}{m!} D^m N_j(t) , \tag{39}$$

where a Taylor's expansion replaced $n_j(t - \delta_{ij})$, that is,

$$n_j(t - \delta_{ij}) = \sum_{m=o}^{\infty} \frac{(-\delta_{ij})^m}{m!} D^m n_j(t) ,$$

and

$$D = \frac{d}{dt} .$$

It is assumed that the two cores are sufficiently similar in composition and geometry that delay times are equal, steady-state coupling coefficients are equal, and generation times are also equal, i.e., $a_o = a_{10} = a_{20}$, since $L = L_1 = L_2$. The possibility still remains, however, that the reactivities

in the two cores may be different. The steady-state condition also yields an expression,

$$r_{io} = -a_{io}n_{jo}/n_{io} ,$$

which when substituted into Equation 39 along with the change in notation,

$$T = n_{20}/n_{10} , \qquad \text{(flux tilt)}$$

give the so-called macrostochastic equations for both regions:

$$(D + a_{10}T)N_1(t) - a_{10}\sum_{m=o}^{\infty}\frac{(-\delta)^m}{m!}D^mN_2(t) = f_1(t)$$

$$- a_{20}\sum_{m=o}^{\infty}\frac{(-\delta)^m}{m!}D^mN_1(t) + (D + a_{10}/T)N_2(t) = f_2(t) , \tag{40}$$

where

$$f_1(t) = n_{10}R_1(t) + n_{20}A_1(t)$$

$$f_2(t) = n_{20}R_2(t) + n_{10}A_2(t) . \tag{41}$$

The derivation of Equation 40 completes the objective of relating the fluctuating variables, $N_1(t)$ and $N_2(t)$ with the fluctuating internal noise sources $R_1(t)$, $R_2(t)$, $A_1(t)$, and $A_2(t)$. This set is in the same form as the general set of Equation 14. In matrix form,

$$ZX = F ,$$

where

$$Z = \begin{pmatrix} D + a_o T & -a_o \sum_{m=o}^{\infty} \frac{(-\delta)^m}{m!} D^m \\ -a_o \sum_{m=o}^{\infty} \frac{(-\delta)^m}{m!} D^m & D + a_o/T \end{pmatrix} ,$$

$$X = \begin{pmatrix} N_1(t) \\ N_2(t) \end{pmatrix} ,$$

and

$$F = \begin{pmatrix} f_1(t) \\ f_2(t) \end{pmatrix} . \qquad (42)$$

Equation 33 is written again for convenience:

$$\Phi_{hk}(\omega) = \sum_{i=1}^{n} \sum_{j=1}^{n} (\underline{Z}^{-1})^*_{hi} \underline{Z}^{-1}_{kj} \Lambda_{ij}(\omega) . \qquad (43)$$

The cross-spectral density function of the fluctuating variables $N_1(t)$ and $N_2(t)$ is

$$\Phi_{12}(\omega) = (\underline{Z}^{-1})^*_{11} \underline{Z}^{-1}_{21} \Lambda_{11}(\omega) + (\underline{Z}^{-1})^*_{12} \underline{Z}^{-1}_{22} \Lambda_{22}(\omega) , \qquad (44)$$

where the other Λ_{ij} are zero because it is assumed that there is no correlation between the fluctuating noise sources $f_p(t)$ and $f_q(t)$, $p \neq q$, that is, application of the definition of Λ_{ij} (Equation 16), would, for example, in the case of $\Lambda_{12}(\omega)$ yield,

$$\Lambda_{12}(\omega) = \int_{-\infty}^{\infty} \lambda_{12}(\tau) e^{-j\omega\tau} d\tau = 0 \ ,$$

since

$$\lambda_{12}(\tau) = \lim_{T\to\infty} \frac{1}{2T} \int_{-T}^{T} f_1(t) f_2(t+\tau) dt = 0 \ .$$

The Fourier transformed Z matrix of Equation 42 becomes

$$\underline{Z} = \begin{pmatrix} j\omega + a_o T & -a_o e^{-j\omega\delta} \\ -a_o e^{-j\omega\delta} & j\omega + a_o/T \end{pmatrix} \ , \qquad (45)$$

and from Equations 34 and 45, $\underline{Z}_{hi}^{-1}$, the h,ith element of the inverse of matrix $\underline{Z}$ is found from

$$\underline{Z}_{hi}^{-1} = \frac{C_{ih}}{\det \underline{Z}} \ ,$$

where C_{ih} is the cofactor of the i,hth element of $\underline{Z}$, and $\det\underline{Z}$ is the determinant of the matrix $\underline{Z}$. Equation 44 is now written in a form which permits direct calculation of the cross-spectral density function of the fluctuating variables $N_1(t)$ and $N_2(t)$, provided the input spectral functions Λ_{11} and Λ_{22} and known.

$$\Phi_{12}(\omega) = \frac{C_{11}^* C_{12}}{|\det\underline{Z}|^2} \Lambda_{11}(\omega) + \frac{C_{12}^* C_{22}}{|\det\underline{Z}|^2} \Lambda_{22}(\omega) \ . \qquad (46)$$

It is assumed in this study that the spectra of the noise inputs are independent of frequency. All that remains is to establish relationships regarding the magnitudes of the

input spectra with respect to steady-state parameters. It is shown in Appendix A that

$$\Lambda_{11} = \frac{n_{10}}{L}\left[1 + \frac{1}{1 + a_o T}\left(\frac{\overline{\nu^2} - 2\bar{\nu}}{\bar{\nu}}\right) + a_o T\right] \tag{47}$$

and

$$\Lambda_{22} = \frac{n_{10} T}{L}\left[1 + \frac{1}{1 + a_o/T}\left(\frac{\overline{\nu^2} - 2\bar{\nu}}{\bar{\nu}}\right) + \frac{a_o}{T}\right] . \tag{48}$$

Equations 47 and 48 are identical if the flux tilt T is unity. After substitution of Equations 47 and 48 into Equation 46 and determination of the cofactors of Equation 46 from Equations 44 and 45, the real part of $\Phi_{12}(\omega)$ is found to be

$$\mathrm{Re}\left[\Phi_{12}(\omega)\right] = \frac{C_1}{|\det \underline{Z}|^2}\left[\Lambda_{11}\left(\frac{a_o}{T}\cos \delta\omega - \omega \sin \delta\omega\right) + \Lambda_{22}\left(a_o T \cos \delta\omega - \omega \sin \delta\omega\right)\right] , \tag{49}$$

and the imaginary part of $\Phi_{12}(\omega)$ is

$$\mathrm{Im}\left[\Phi_{12}(\omega)\right] = \frac{-C_1}{|\det \underline{Z}|^2}\left[\Lambda_{11}\left(\frac{a_o}{T}\sin \delta\omega + \omega \cos \delta\omega\right) - \Lambda_{22}\left(a_o T \sin \delta\omega + \omega \cos \delta\omega\right)\right] , \tag{50}$$

where

$$\det \underline{Z} = a_o^2(1 - \cos 2\,\delta\omega) - \omega^2 + j a_o\left[\omega(T + 1/T) + a_o \sin 2\,\delta\omega\right] , \tag{51}$$

and C_1 is a constant.

When the flux tilt is set equal to one, $\Lambda_{11} = \Lambda_{22}$, and Equation 49 may be written as

$$\mathrm{Re}[\Phi_{12}(\omega)] = \frac{C_2}{|\det \underline{Z}|^2}(a_o \cos \delta\omega - \omega \sin \delta\omega) \ . \qquad (52)$$

It is obvious that the real part of Φ_{12} vanishes when the terms in the parentheses are equal. The frequency at which the real part of the cross-spectral density function vanishes is called the sink frequency, and for convenience it is denoted by the symbol ω_s. Thus, for the special case of T = 1,

$$a_o = \omega_s \tan \delta\omega_s . \qquad (53)$$

Under the conditions of the assumed model, it is possible to determine the ratio of the coupling reactivity to generation time, $a_o = \alpha_o/L$, in terms of the delay time and sink frequency. Although only the special case of T = 1 has been considered here, it can be shown that the real part of the cross-spectral density function vanishes at the sink frequency for all values of flux tilt. Previous investigators (7, 11) have shown experimentally that the delay time of a disturbance propagated through a nonmultiplying medium is to a good approximation determined from the velocity of a neutron wave. The wave velocity as given by Danofsky (11) is

$$V = \omega \left\{ \frac{2}{\left[F^4 + \left(\frac{\omega}{vD}\right)^2\right]^{1/2} - F^2} \right\}^{1/2} \tag{54}$$

where

ω is the angular frequency, (rad/sec)

$F^2 = (\pi/a)^2 + (\pi/b)^2 + (1/L)^2$; a and b are the transverse dimensions of the medium and L is the diffusion length,

v is the neutron velocity, and

D is the diffusion coefficient.

The delay time is then equal to the propagation distance divided by the wave velocity. Curves representing values of α_o/L as a function of sink frequency with propagation distance as a parameter are shown in Figure 1. The sensitivity of the function in Equation 53 to variations in delay time is clearly shown in Figure 1. It is therefore important that care be exercised in the determination of the propagation distance.

In this investigation, the vanishing character of the real part of the cross-spectral density was verified experimentally for the first time. However, the experimental conditions deviated from those proposed in the First Model, since it was not possible to observe the fluctuating variables $N_1(t)$ and $N_2(t)$ independently. Neutron detectors were positioned in experimental access locations adjacent to the cores as shown in Figure 2. In the Second Model, which

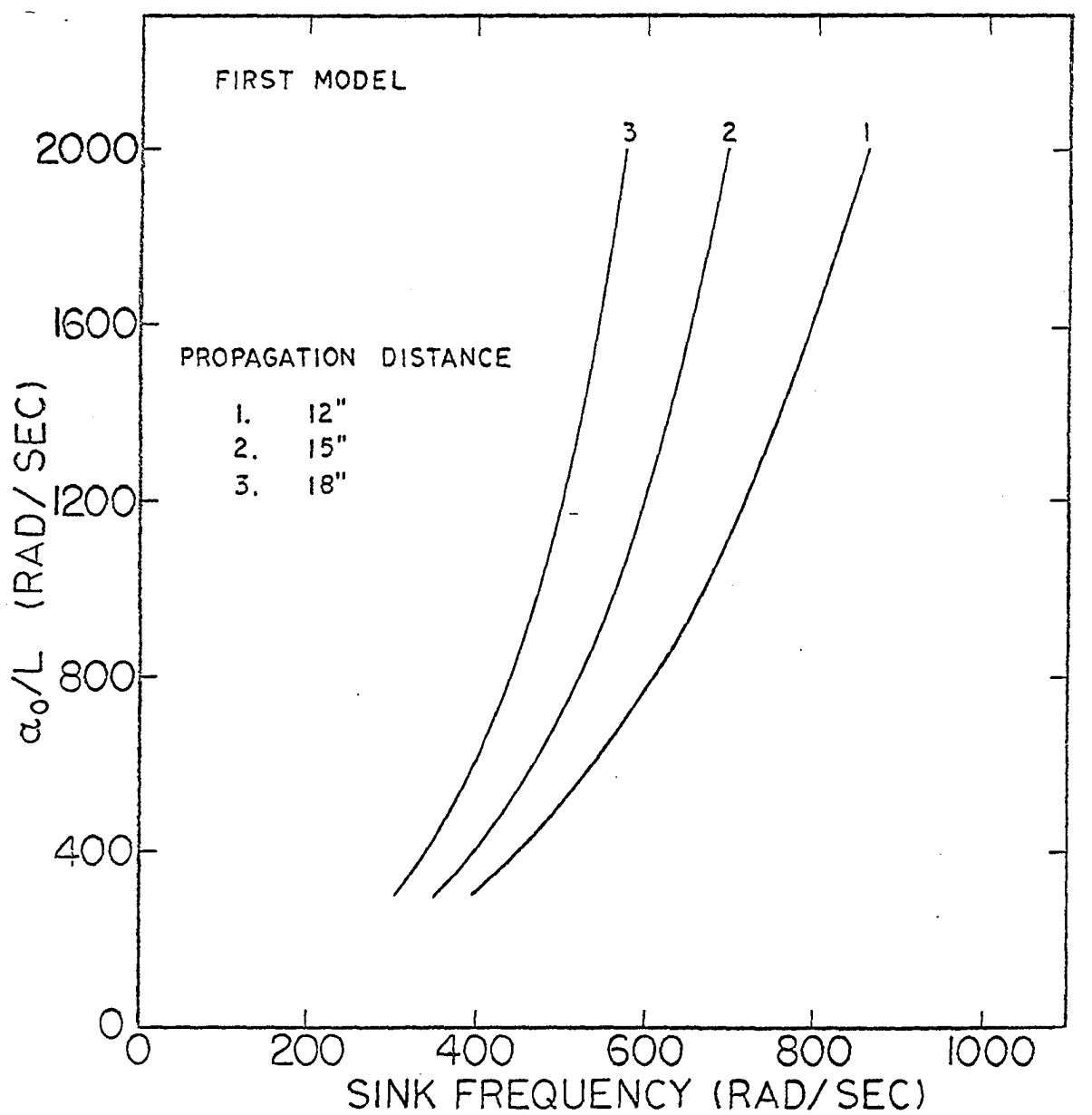

Figure 1. First Model. α_o/L versus ω_s with propagation distance as a parameter, (a = 44 inches, b = 48 inches).

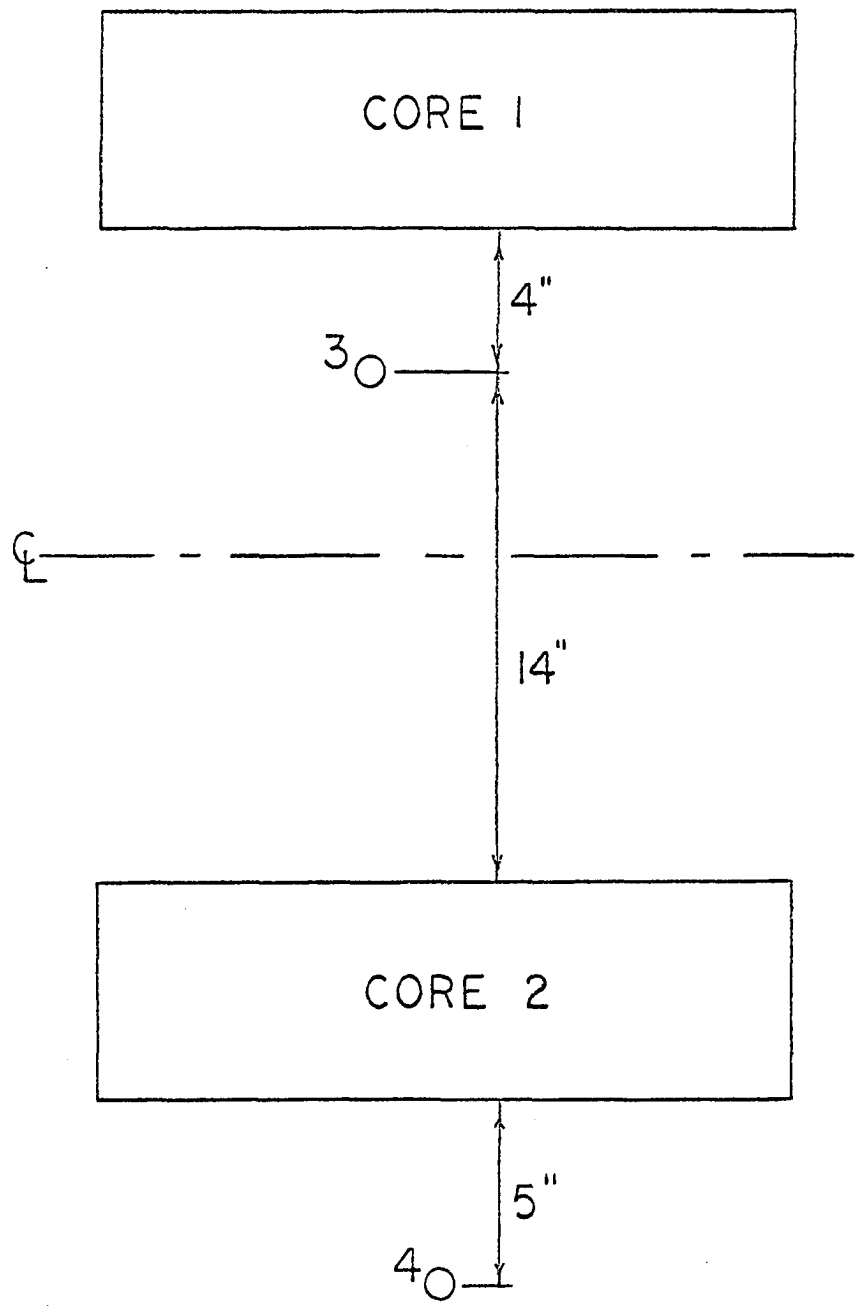

Figure 2. Detector locations 3 and 4 in the UTR-10 reactor.

follows, the expressions needed to determine the cross-spectral density function of the neutron density fluctuation at the detector locations are derived.

2. Second Model

The rate of change of neutron density at point 3 is

$$\frac{dn_3(t)}{dt} = \frac{k_{13}}{L} n_1(t - \delta_{13}) + \frac{k_{23}}{L} n_2(t - \delta_{23}) - \gamma n_3(t), \quad (55)$$

where the first two terms on the right hand side represent the gain in neutron density per generation at point 3 due to delayed, attenuated disturbances originating in the cores. The last term on the right states that the loss at point 3 is proportional to the neutron density there, the constant of proportionality being γ. It will be shown later that an approximate value of γ may be obtained from a suitable match of theoretical and experimental curves, and that the value of γ affects only the shape of the cross-spectrum in the neighborhood of the sink frequency and not the sink frequency itself.

The neutron density at point 4 changes at a rate given by

$$\frac{dn_4(t)}{dt} = \frac{k_{24}}{L} n_2(t - \delta_{24}) - \gamma n_4(t) , \quad (56)$$

where the gain in neutron density per generation at point 4 is due to delayed, attenuated disturbances originating in

core 2, only. The proportionality constant γ is assumed to be identical at points 3 and 4, since the physical properties of the medium at the detector locations are approximately equal.

An expression for the amplitude attenuation of a neutron wave traveling in a non-multiplying medium is

$$A = A_o \exp(-x/a) \tag{57}$$

where x is the propagation distance and a is the attenuation length of the wave (25). In terms of the parameters used previously in Equation 54, the attenuation length is given by

$$a = \left\{ \frac{2}{\left[F^2 + \left(\frac{\omega}{vD}\right)^2\right]^{1/2} + F^2} \right\}^{1/2} . \tag{58}$$

It is evident that the k_{ij}, (i = 1,2.; j = 3,4.), in Equations 56 and 57 are frequency dependent and are given by

$$k_{ij} = \exp(x_{ij}/a) , \tag{59}$$

where x_{ij} is the appropriate propagation distance. The fluctuation equation may be derived from Equations 55 and 56 based on the assumptions that the parameter γ does not fluctuate and steady-state values of the attenuation factors do not exist. With the aid of previously introduced notation, the fluctuations of $N_3(t)$ and $N_4(t)$ are expressed as

$$DN_3(t) = \frac{k_{13}}{L}\sum_{m=o}^{\infty}\frac{(-\delta_{13})^m}{m!}D^mN_1(t) + \frac{k_{23}}{L}\sum_{m=o}^{\infty}\frac{(-\delta_{23})^m}{m!}D^mN_2(t) - \gamma N_3(t) \tag{60}$$

and

$$DN_4(t) = \frac{k_{24}}{L}\sum_{m=o}^{\infty}\frac{(-\delta_{24})^m}{m!}D^mN_2(t) - \gamma N_4(t) \ . \tag{61}$$

The coupled set of fluctuation equations, written in the form of Equation 14 are

$$\begin{aligned}
&(D + a_oT)N_i(t) - a_o\sum_{m=o}^{\infty}\frac{(-\delta_{12})^m}{m!}D^mN_2(t) = f_1(t)\\
&-a_o\sum_{m=o}^{\infty}\frac{(-\delta_{12})^m}{m!}D^mN_1(t) + (D + a_o/T)N_2(t) = f_2(t)\\
&-K_{13}\sum_{m=o}^{\infty}\frac{(-\delta_{13})^m}{m!}D^mN_1(t) - K_{23}\sum_{m=o}^{\infty}\frac{(-\delta_{23})^m}{m!}D^mN_2(t)\\
&+ (D + \gamma)N_3(t) = f_3(t)\\
&-K_{24}\sum_{m=o}^{\infty}\frac{(-\delta_{24})^m}{m!}D^mN_2(t) + (D + \gamma)N_4(t) = f_4(t)
\end{aligned} \tag{62}$$

where $K_{13} = k_{13}/L$, etc., and $f_3(t) = f_4(t) = 0$.

The Fourier transformed matrix, $\underline{Z}$, becomes

$$\underline{Z} = \begin{pmatrix} j\omega + a_o T & -a_o \exp(-j\omega\delta_{12}) & 0 & 0 \\ -a_o \exp(-j\omega\delta_{12}) & j\omega + a_o/T & 0 & 0 \\ K_{13}\exp(-j\omega\delta_{13}) & K_{23}\exp(-j\omega\delta_{23}) & -D-\gamma & 0 \\ 0 & K_{24}\exp(-j\omega\delta_{24}) & 0 & -D-\gamma \end{pmatrix} \tag{63}$$

The expression for the cross-spectral density function of the fluctuating variables $N_3(t)$ and $N_4(t)$ in terms of the matrix elements is

$$\Phi_{34}(\omega) = (\underline{Z}^{-1})^*_{31}\underline{Z}^{-1}_{41}\Lambda_{11} + (\underline{Z}^{-1})^*_{32}\underline{Z}^{-1}_{42}\Lambda_{22} \; . \tag{64}$$

The real and imaginary components of Φ_{34}, calculated from Equations 34, 63, and 64, are

$$\begin{aligned} \mathrm{Re}[\Phi_{34}(\omega)] = \frac{C_3}{|\det\underline{Z}|^2}(\omega^2 + \gamma^2)K_{24}\Big\{ & \Lambda_{11}\Big[a_o^2 K_{23}\cos(\delta_{23} - \delta_{24})\omega \\ & + \frac{a_o^2}{T}K_{13}\cos(\delta_{12} - \delta_{13} + \delta_{24})\omega \\ & - a_o\omega K_{13}\sin(\delta_{12} - \delta_{13} + \delta_{24})\omega\Big] \\ & + \Lambda_{22}\Big[K_{23}(\omega^2 + a_o^2T^2)\cos(\delta_{23} - \delta_{24})\omega \\ & + a_o K_{13}\Big\{a_o T\cos(\delta_{12} + \delta_{13} - \delta_{24})\omega \\ & - \omega\sin(\delta_{12} + \delta_{13} - \delta_{24})\omega\Big\}\Big]\Big\} \quad , \end{aligned} \tag{65}$$

and

$$\mathrm{Im}[\Phi_{34}(\omega)] = \frac{C_3}{\det\underline{Z}^2}(\omega^2 + \gamma^2)K_{24}\Big\{\Lambda_{11}\Big[a_o^2K_{23}\sin(\delta_{23} - \delta_{24})\omega$$

$$+ a_o^2K_{13}\sin(\delta_{12} - \delta_{13} + \delta_{24})\omega$$

$$- a_o\omega K_{13}\cos(\delta_{12} - \delta_{13} + \delta_{24})\omega\Big]$$

$$+ \Lambda_{22}\Big[K_{23}(\omega^2 + a_o^2T^2)\sin(\delta_{23} - \delta_{24})\omega$$

$$+ a_oK_{13}\Big\{a_oT\sin(\delta_{12} + \delta_{13} - \delta_{24})\omega$$

$$- \omega\cos(\delta_{12} + \delta_{13} - \delta_{24})\omega\Big\}\Big]\Big\}, \qquad (66)$$

where

$$\det\underline{Z} = (\gamma^2 - \omega^2)(a_o^2 - \omega^2 - a_o^2\cos 2\delta_{12}\omega) - \omega\gamma\Big[\omega a_o(T + 1/T)$$

$$+ a_o^2\sin 2\delta_{12}\omega\Big] + j\Big\{(\gamma^2 - \omega^2)\Big[\omega a_o(T + 1/T)$$

$$+ a_o^2\sin 2\delta_{12}\omega\Big] + \omega\gamma(a_o^2 - \omega^2 - a_o^2\cos 2\delta_{12}\omega)\Big\}, \qquad (67)$$

and C_3 is a constant.

The real part of $\Phi_{34}(\omega)$ vanishes at the sink frequency, exhibiting a behavior similar to $\mathrm{Re}\left[\Phi_{12}(\omega)\right]$ in the First Model. The sink frequencies of the Second Model are approximately 200 rad/sec greater than those of the First Model for identical values of α_o/L. Curves of α_o/L plotted as a function of sink frequency are shown in Figure 3. Two of the three propagation distances represent increased effective size of the core regions while the detector locations remain

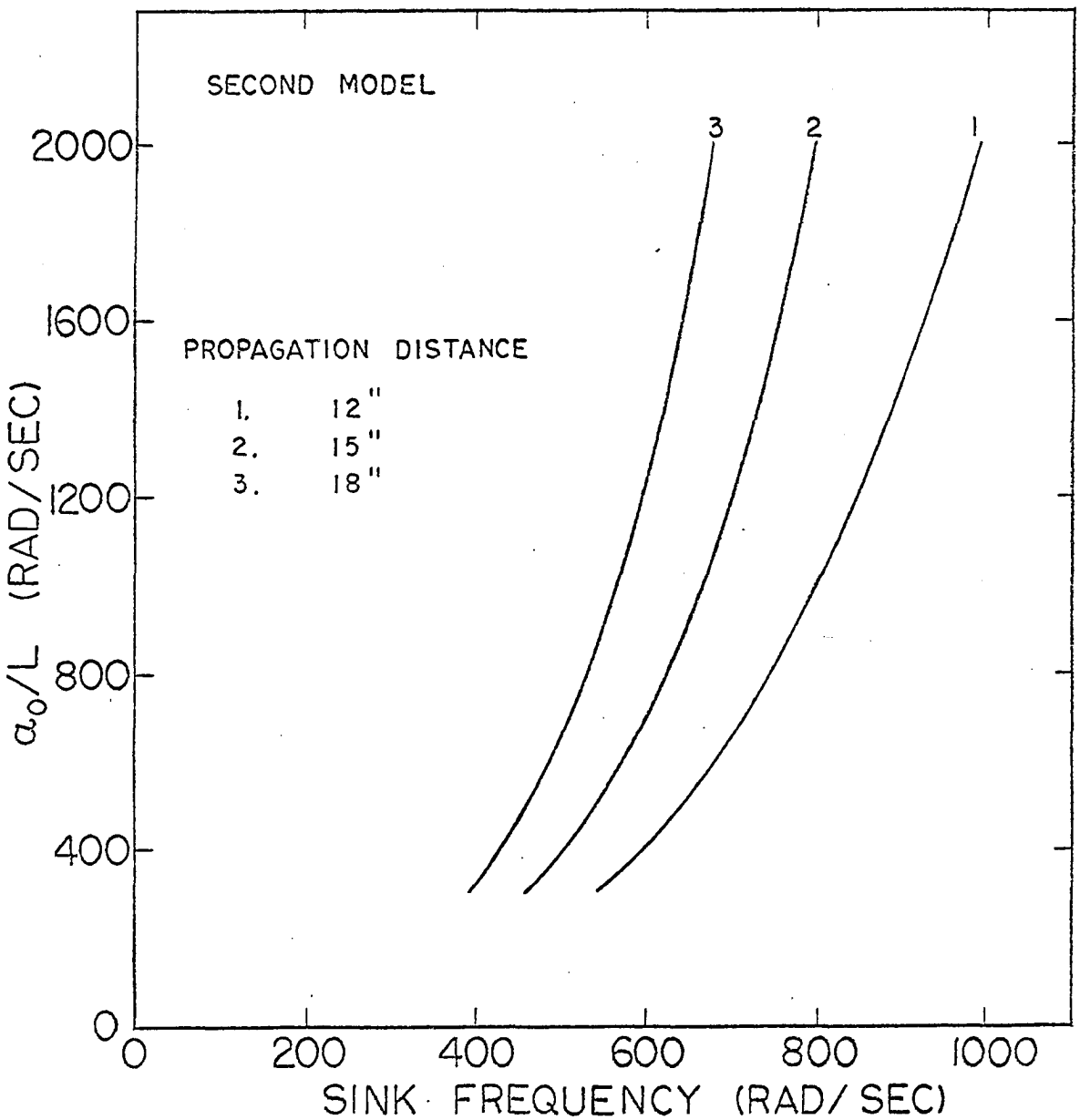

Figure 3. Second Model. α_o/L versus ω_s with propagation distance as a parameter, (a = 44 inches, b = 48 inches).

unaltered with respect to the center line shown in Figure 2. The modification of the core size, in effect, changes the bare, point reactors to reflected, point reactors with reduced propagation distances. At constant sink frequency, the curves of Figure 3 clearly show that small changes in propagation distance cause large variations in the value of α_o/L.

IV. EXPERIMENTAL INVESTIGATION

The techniques of recording and analyzing reactor noise data fall into two basic categories: (1) Digital or discrete, and (2) analog or continuous methods. Certain unique advantages are associated with each method, but the choice of approach usually depends primarily upon the experimental or theoretical requirements of the model under investigation and the availability of equipment needed to perform the analysis. In this investigation, a combination of both requirements led to the choice of the analog method.

A. Theory of Cross-spectral Density Measurements

The crosscorrelation function is not an even function of the lag interval, and hence, the cross-spectral density function is generally a complex number,

$$\Phi_{xy}(\omega) = C_{xy}(\omega) - jQ_{xy}(\omega) \ , \tag{13}$$

where the real part is the co-spectral density function, and the quadrature spectral density function is the imaginary part. A brief examination of the development of the co-spectral and quadrature spectral density functions in terms of the experimental variables follows.

The crosscorrelation function was defined in Equation 10 and related to the cross-spectral density function by the

Fourier transform, so that

$$\varphi_{xy}(\tau) = \frac{1}{2\pi}\int_{-\infty}^{\infty} \Phi_{xy}(\omega)e^{j\omega\tau}d\omega \ . \tag{11}$$

It is convenient to consider the relation

$$\lim_{T\to\infty} \frac{1}{T} \int_{o}^{T} x(t,\omega_o,\Delta\omega)y(t + \tau,\omega_o,\Delta\omega)dt =$$

$$\frac{1}{2\pi} \int_{\omega_o}^{\omega_o + \Delta\omega} \Phi_{xy}(\omega_o,\Delta\omega)e^{j\omega_o\tau}d\omega \ , \tag{68}$$

where $x(t,\omega_o,\Delta\omega)$ and $y(t + \tau,\omega_o,\Delta\omega)$ are filtered portions of $x(t)$ and $y(t)$ in a narrow frequency interval between ω_o and $\omega_o + \Delta\omega_o$. If the cross-spectral density at ω_o, $\Phi_{xy}(\omega_o,\Delta\omega)$, is constant over the frequency interval, the right hand side of Equation 68 becomes

$$\frac{1}{2\pi}\Phi_{xy}(\omega_o)e^{j\omega_o\tau}{}_{\Delta\omega}. \tag{69}$$

The Euler relation is used in Equation 69 to obtain

$$\frac{1}{2\pi}\Phi_{xy}(\omega_o)(\cos\ \omega_o\tau + j\ \sin\ \omega_o\tau)\Delta\omega \ , \tag{70}$$

and since Φ_{xy} is complex,

$$\lim_{T\to\infty} \frac{1}{T} \int_{o}^{T} x(t,\omega_o,\Delta\omega)y(t + \tau,\omega_o,\Delta\omega)dt = \frac{1}{2\pi}\Big[C_{xy}(\omega_o)\ \cos\omega_o\tau$$

$$- Q_{xy}(\omega_o)\sin\omega_o\tau + j(C_{xy}(\omega_o)\sin\omega_o\tau + Q_{xy}(\omega_o)\cos\omega_o\tau)\Big] \ , \tag{71}$$

where C_{xy} and Q_{xy} are the real and imaginary parts, respectively, of the cross-spectral density function. When the lag interval τ is set equal to zero, Equation 71 reduces to

$$C_{xy}(\omega_o) = \frac{2\pi}{\Delta\omega} \lim_{T\to\infty} \frac{1}{T} \int_o^T x(t,\omega_o,\Delta\omega)y(t,\omega_o,\Delta\omega)dt \ , \qquad (72)$$

since the left hand side of Equation 71 is a real quantity. When $\tau = \pi/2\omega_o$, it follows that

$$Q_{xy}(\omega_o) = \frac{2\pi}{\Delta\omega} \lim_{T\to\infty} \frac{1}{T} \int_o^T x(t,\omega_o,\Delta\omega)y(t + \frac{\pi}{2\omega_o},\omega_o,\Delta\omega)dt \ . \qquad (73)$$

Therefore, the co-spectral density function, in terms of frequency, is the average product of the filtered variables, $x(t)$ and $y(t)$, divided by the frequency interval. Similarly, the quadrature spectral density is the average product of $x(t)$ and the 90-degree shifted variable, $y(t + \frac{\pi}{2\omega_o})$, divided by the frequency interval.

The true average product of two stationary, ergodic random signals can only be estimated in practice since the averaging time must be of finite duration. Hence, the notation and form of Equations 13, 72, and 73 are modified to emphasize that the resulting expressions are estimates derived from finite sampling time.

$$\hat{\Phi}_{xy}(\omega_o) = \hat{C}_{xy}(\omega_o) - j\hat{Q}_{xy}(\omega_o) \qquad (74)$$

$$\hat{C}_{xy}(\omega_o) = \frac{2\pi}{(\Delta\omega)T} \int_o^T x(t,\omega_o,\Delta\omega)y(t,\omega_o,\Delta\omega)dt \qquad (75)$$

$$\hat{Q}_{xy}(\omega_o) = \frac{2\pi}{(\Delta\omega)T} \int_o^T x(t,\omega_o,\Delta\omega)y(t + \frac{\pi}{2\omega_o},\omega_o,\Delta\omega)dt \; . \qquad (76)$$

The cross-spectral density is estimated by (1) passing the signals x(t) and y(t) through identical, narrow band-pass filters set at the same center frequency and bandwidth, (2) continuously multiplying the unshifted, filtered signals, (3) continuously multiplying the unshifted, and 90-degree-shifted, filtered signals, (4) averaging the products formed in (2) and (3) over the finite sampling time, and (5) dividing each of the averaged products by the bandwidth. The block diagram in Figure 4 illustrates these operations. A complete spectrum of values of $\hat{C}_{xy}$ and $\hat{Q}_{xy}$ as a function of frequency can be obtained by selecting different settings of the center frequency throughout the frequency range of interest.

B. Equipment and Procedures

The measurement of the cross-spectral density function was performed in two separate operations. First, wide-band reactor noise signals were recorded on magnetic tape, then the data stored on the magnetic tape were analyzed as a function of frequency at a later time. Functional block diagrams illustrating the recording and analyzing systems

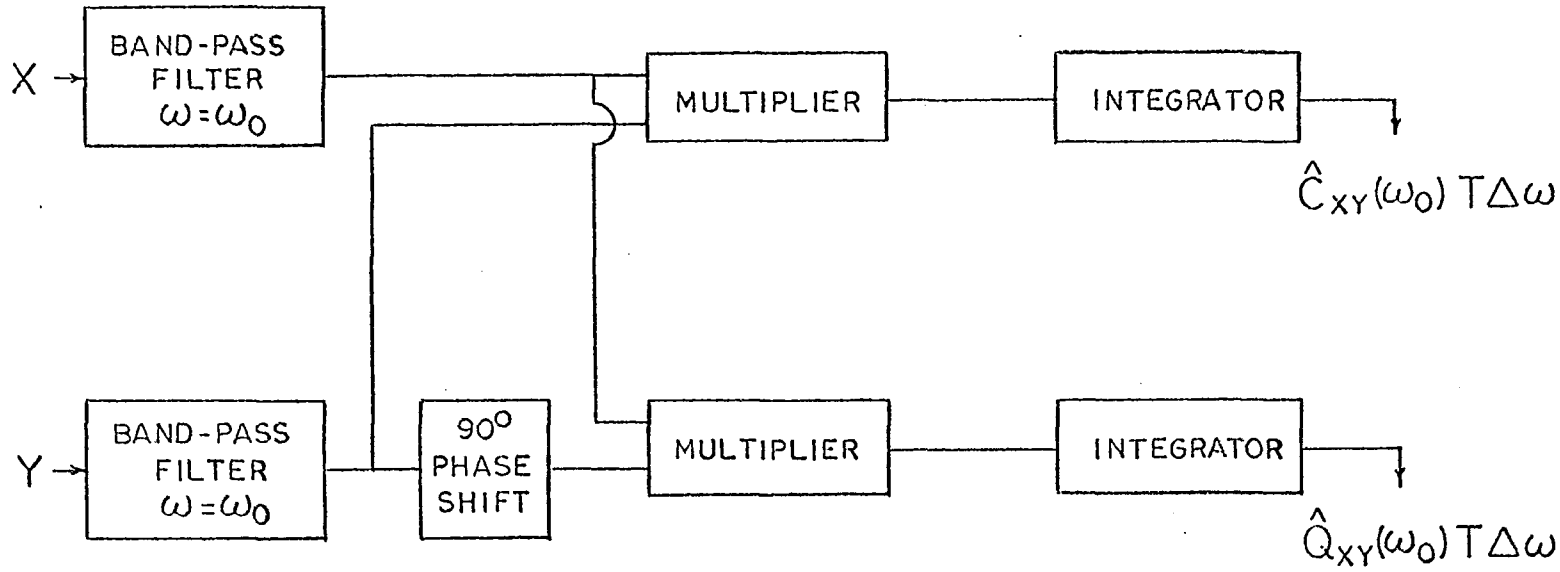

Figure 4. Block diagram of cross-spectral density analyzer.

are presented in Figure 5.

Two BF_3 gas-filled neutron detectors (1-inch in diameter by 4-inch active length) were positioned at the midplane of the reactor in the graphite reflector region, shown in Figure 2 as points 3 and 4. Each detector was connected to a small preamplifier by a 24-inch cable. The cable and detector were mounted in machined graphite holders to minimize the loss of reflector material. The preamplifier acted as a conventional cathode follower circuit by matching the detector-cable and pulse amplifier impedences and preserving the negative polarity of the pulses produced in the detector. Pulses from the preamplifiers were amplified and shaped in pulse amplifiers. High voltage was supplied to each detector, through its preamplifier, from a power supply section in the pulse amplifier chassis.

The output pulses from each pulse amplifier were fed to a count-rate circuit, where the pulse-type signals were converted to continuous voltage fluctuations. Proportionality between the rate of arrival of pulses at the input to the counting-rate circuit and the mean level of the output voltage was experimentally verified over a range of reactor power spanning the power level at which measurements were performed. It was thus assumed that the fluctuating voltage (about the mean) at the count-rate circuit output was, to a reasonable approximation, linearly related to the

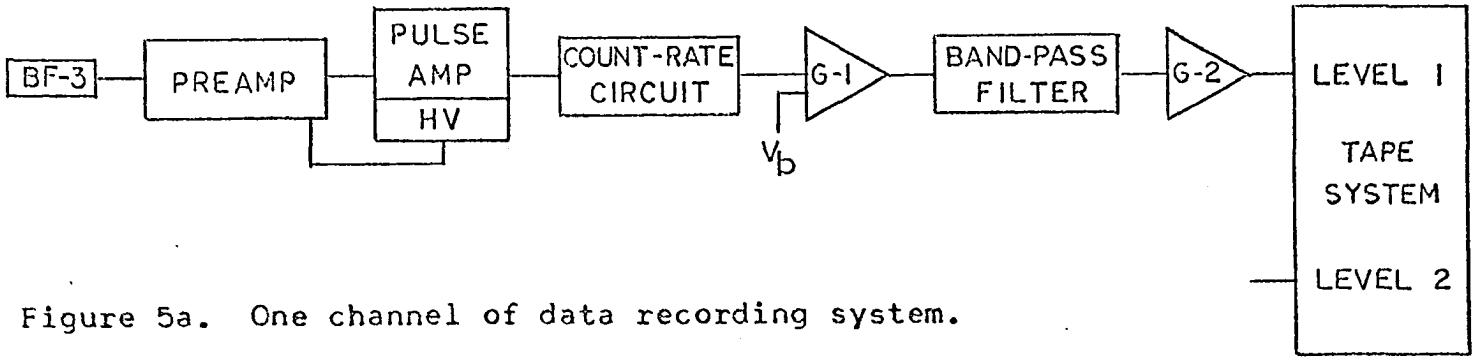

Figure 5a. One channel of data recording system.

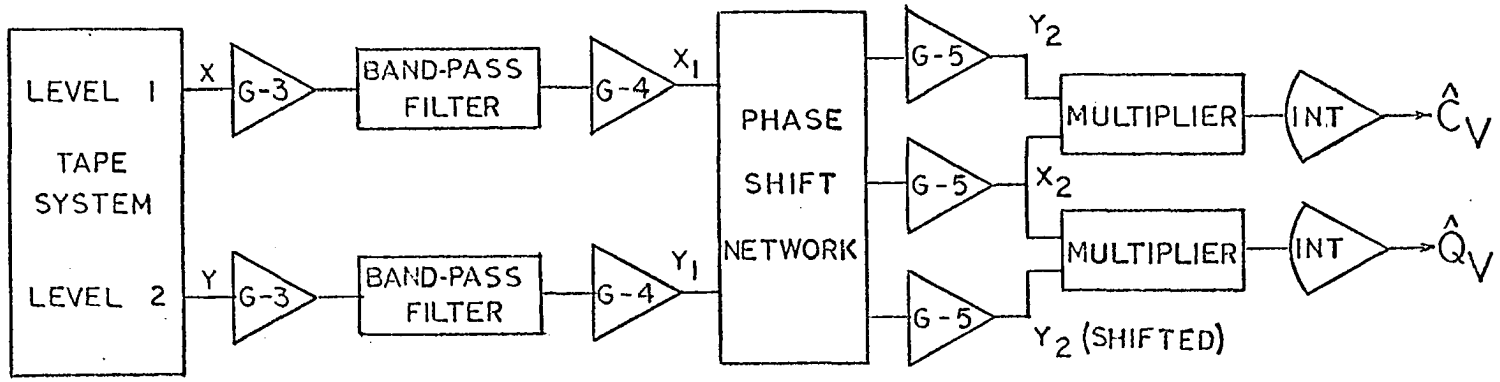

Figure 5b. Data analyzing system.

fluctuation of the neutron density at the detector location.

The count-rate circuit was designed to operate on the diode-pump principle with the passive elements chosen so that the frequency response curve passed through the -3 db point at approximately 15 cps, and the circuit voltage fluctuations attained a maximum value of approximately 10 millivolts peak to peak. In addition, the standard count-rate circuit design criteria (21) were also satisfied.

The mean level of the output voltage of each count-rate circuit was cancelled with a bucking voltage applied to the input of an operational amplifier, and the fluctuating voltage amplitude was boosted before the signal entered the band-pass filter. Each band-pass filter, with a frequency response of -24 decibels per octave on both ends of the pass band, was set at 0.1 cps low cutoff and 1000 cps high cutoff.

The filtered signals were amplified to approximately one volt r.m.s., frequency modulated, and recorded on two levels of magnetic tape. A tape speed of 7½ inches per second was selected for the data recording operation.

Reactor power was manually controlled and held constant at approximately one milliwatt. Experimental data were recorded and later analyzed.

The data analyzing system originated with the stored data being reproduced by the F.M. tape unit. The playback

tape speed was one and seven-eighths inches per second, one-fourth of the recording speed. This speed reduction increased the analyzer resolution by a factor of four without significantly increasing the variance portion of the statistical error.

Amplified signals from the tape recorder unit were fed to separate band-pass filters. A minimum band width was obtained by tuning the high and low cutoff frequency controls to the same value which was the center frequency. When the high and low cutoff frequencies were equal to f_1, the half-power (-3 db) points were located at $0.77f_1$, and $1.30f_1$, respectively. Therefore, the bandwidth was a constant percentage of the center frequency. The center frequencies of the two filters were compared by feeding a sinusoidal test voltage to the filters and observing the Lissajous' patterns of the output voltage wave forms on a dual beam oscilloscope. The center frequencies of the filters were adjusted, in turn, until a zero phase shift between the output signals of the two filters was observed.

Amplified narrow-band signals were fed to the phase-shifting network. This network was composed of adjustable high-pass and low-pass filters which were tuned so that the three output signals (under test signal conditions) were of equal amplitude and one output signal led the two in-phase

signals by 90-degrees. A tuning procedure similar to that used on the band-pass filters was applied to the phase shifting network.

Quarter-square, electronic multipliers were used to form appropriate products of the shifted and unshifted signals from the phase shifting network. Separate, stable power supplies provided bias voltages to the multiplier circuits so that 0.1 percent accuracy was achieved in the multiplication of test voltages. Accurate calibration of the multipliers was extremely important in order to obtain accurate estimates of the real part of the cross-spectral density in the neighborhood of the sink frequency.

The multiplied signals were integrated for five minutes, and the voltages representing the real and imaginary parts of the cross-spectral density were measured with a null voltmeter. A conservative estimate of the integrator voltage measurement error was ± 0.01 volt.

Cross-spectral density estimates were obtained at selected center frequencies covering the frequency range of 10 cps to 200 cps.

The precision of the spectral analyzing system and the frequency response of the count-rate circuit were determined by measuring the transfer function and the cross-spectral density function, respectively, between the input and output signals of two different low-pass filters

constructed from precision components. Signals generated in a single BF_3 detector exposed to a Pu-Be neutron source and subsequently processed through a count-rate circuit served as the input to the low-pass filters.

The precision of the system was checked by measuring the transfer function of a low-pass filter with a 32 cps break frequency. When normalized, measured and calculated values were within ½ db in magnitude and 2-degrees in phase angle.

The frequency response of each counting-rate circuit was obtained by measuring the magnitude of the cross-spectral density function between the input and output of a low-pass filter with a 320 cps break frequency. The measured values were corrected to remove the effect of the low-pass filter in the high frequency region. The frequency response curve of the analyzing system is shown in Figure 6. The data were normalized with respect to the 10 cps measurement.

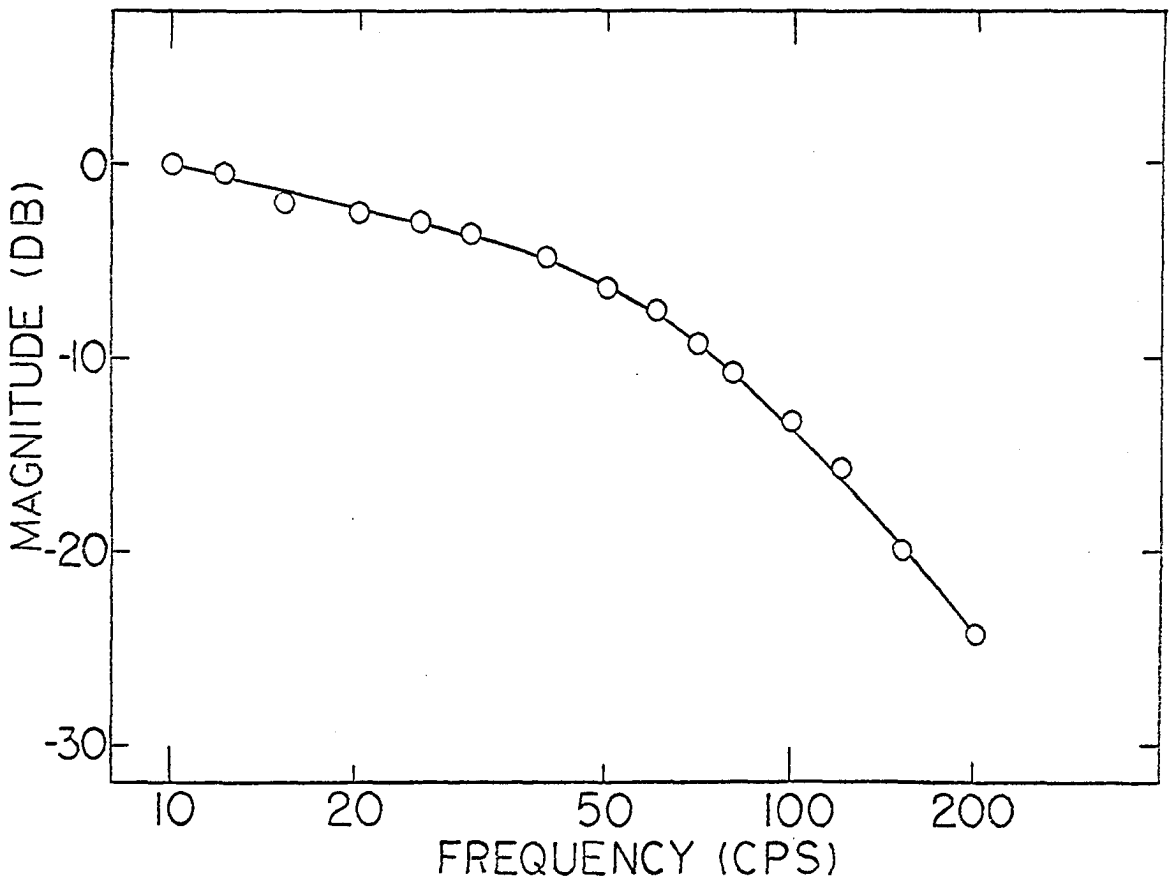

Figure 6. Frequency response of the counting-rate circuit.

V. RESULTS

The unusual behavior of the cross-spectral density function was first observed during experimental measurements performed in the early stages of this investigation. The literature contained no reported results of similar character. In order to substantiate the observed results, a theoretical model was developed which predicted that the magnitude of the cross-spectral density function would change rapidly in the neighborhood of the sink frequency.

The estimate of the cross-spectral density function of the neutron density fluctuations at points 3 and 4 in the reactor for two experimental runs is shown in Figure 7. The flags on the data points represent normalized standard errors. An analysis of the experimental errors appears in Appendix B. The influence of the frequency response of the analyzing system on the measured function was removed by applying magnitude corrections (obtained from Figure 6) at the appropriate frequency. The data were normalized to the 10 cps measurement of run number one and plotted in the conventional form of 10 log magnitude ratio versus log frequency. The prescription "10 log ratio" is applicable since the measurements represent the product of input voltages.

A theoretical expression for the magnitude of the cross-spectral density function, derived from Equations 65, 66, and 67, was plotted with the experimental data in Figure 7 so

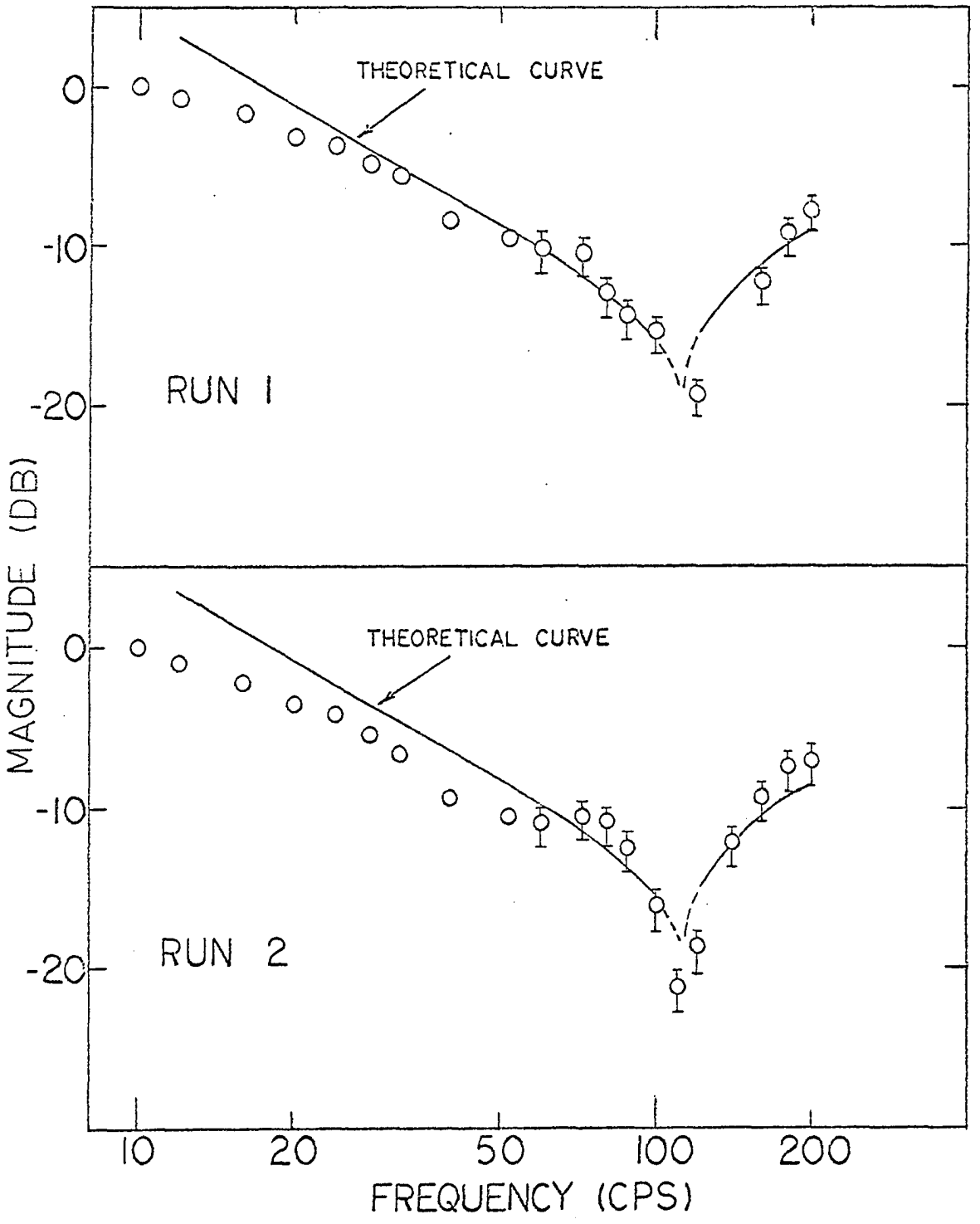

Figure 7. Cross-spectral density function, $\Phi_{34}(\omega)$, for two experimental runs.

that the frequencies at which the real parts of the measured and theoretical spectral density functions vanished would approximately coincide. The theoretical data were obtained from calculations performed on a digital computer where parametric values of α_o/L, propagation distance, and γ (from Equations 55 and 56) were tested until the best fit of the experimental curve was established.

The most prominent characteristic of the cross-spectral density function is the rapid loss and subsequent recovery of magnitude in the neighborhood of the sink frequency. This behavior implies that the fluctuations of the neutron density at the detector locations become approximately uncorrelated at the sink frequency. Hence, the coupling interaction decreases to a minimum value at a particular frequency. The coupling interaction increases rapidly as the frequency increases beyond ω_s and then approaches an apparent relative maximum value at the upper limit of the frequency range investigated.

In the low frequency region, the theoretical curve deviates from the experimental data as frequency decreases. Although the model is not able to describe accurately the low frequency behavior of the cross-spectral density function, the agreement of theory and experiment in the neighborhood of the sink frequency is adequate to demonstrate this method of estimating the ratio of reactivity coupling coefficient to

generation time in a coupled-core reactor.

A plot of the cross-spectral density function with γ as a parameter is presented in Figure 8. These curves show that the value of γ, which was of minor interest in this study, does not affect the predicted sink frequency. However, the shape of the theoretical curve changes when γ is varied. An approximate value of $\gamma = 1.0$ was determined by adjusting this parameter until the theoretical curve conformed reasonably with the shape of the measured spectral density function.

The flux tilt, which represents the ratio of steady-state neutron density in core two to core one, was assumed to be equal to unity in all calculations since the magnitude of the cross-spectral density function is known to be insensitive to small changes in flux tilt. It has been shown (12, 18) that the flux tilt in the UTR-10 does not exceed $T = 1.2$. According to Leribaux (18), a maximum error of less than 1.5 percent would be expected if the flux tilt was assumed to be equal to unity.

The influence of the parameters α_o/L and propagation distance on the predicted sink frequency was established in Section III and illustrated in Figures 1 and 3. An experimental value of α_o/L may be determined from Figure 3 when the measured sink frequency and propagation distance are known. Measured delay times between the cores and between

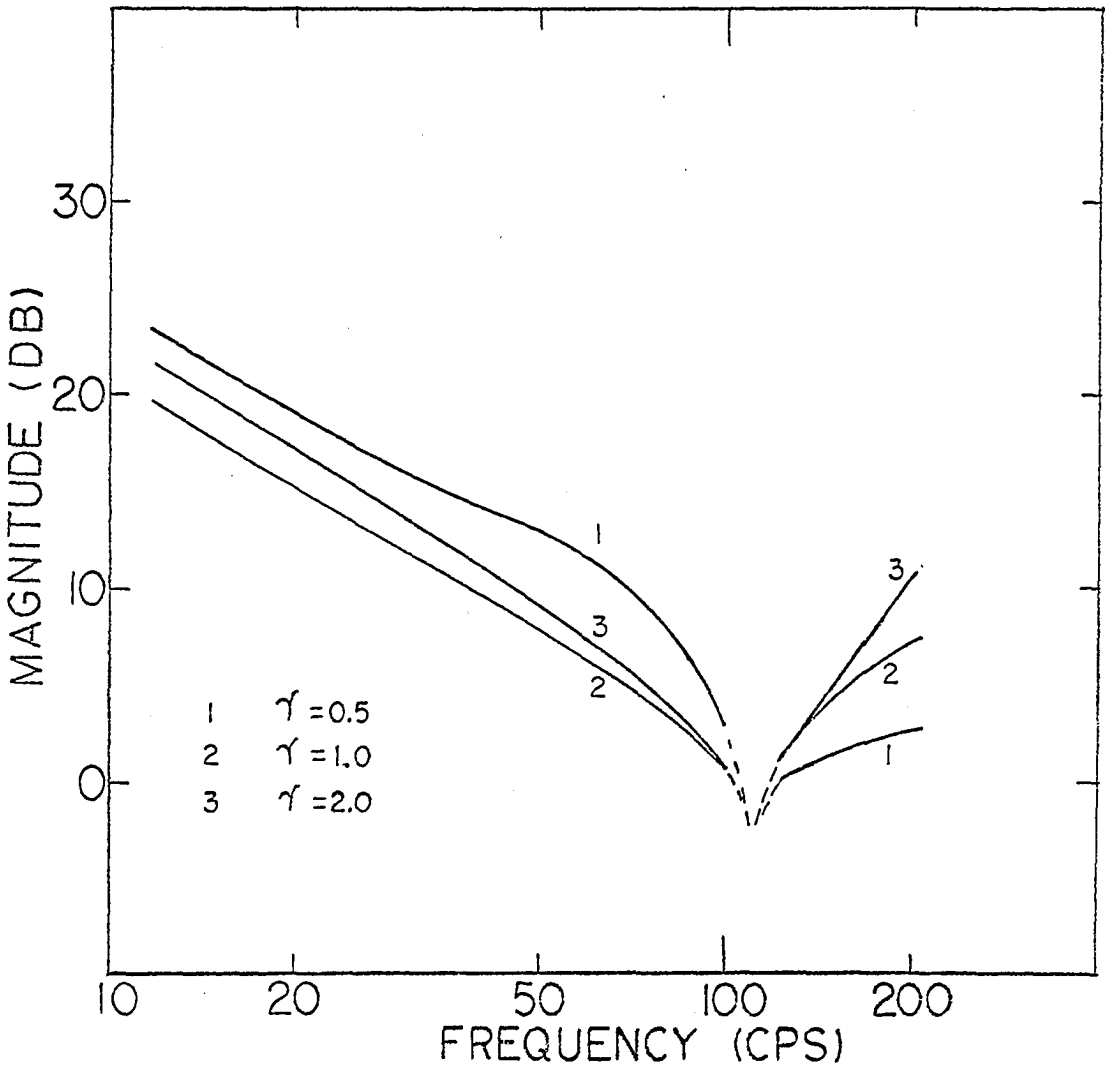

Figure 8. Magnitude of cross-spectral density function with γ as a parameter.

the cores and detectors were not available, so theoretical values of the delay times were calculated using the wave velocity model. An approximation of the propagation distance between cores was taken to be equal to the separation distance less the reflector savings associated with each reflected core. The calculated reflector savings for each reflected core was found to be approximately 1.5 inches, and hence, the propagation distance between cores was taken as 15 inches. The value of α_o/L obtained from Figure 3 (based on ω_s = 115 ± 5 cps and propagation distance = 15 inches) was

$$\frac{\alpha_o}{L} = 1360 \pm 220 \frac{\text{rad}}{\text{sec}} .$$

A value of the reactivity coupling coefficient, α_o, can be found by using a value of $L = 5 \times 10^{-5}$ seconds. This value of the mean generation time was estimated from a crude calculation of the reciprocal destruction rate in either core. (Destruction rate and production rate are approximately equal in the cores.) The prompt neutron lifetime calculated by the designer of the UTR-10 reactor is 1.35×10^{-4} seconds (based on a one-dimensional, two group approximation), however, the calculation takes into account the destructive processes occuring in the total reactor system. In this investigation, attention was focused on the cores as separate entities with propagated neutron-wave disturbances

between the cores serving as the coupling interaction required to sustain critical operation. The reactivity coupling coefficient is

$$\alpha_o = 0.068 \pm 0.011 \ .$$

This value of α_o is larger than that given by the designer of the UTR-10. The manufacturer's value of $\alpha_o = 0.0155$ was obtained from estimates of the reactivity equivalent of additional fuel required to attain single-core, critical operation. It is well known that such estimates derived from critical experiments are subject to large uncertainties, hence, the measured value of α_o (during critical operation) is preferred.

It is interesting to compare reported values of the reactivity coupling coefficient of two other coupled-core reactors. Baldwin (3) reported a value of $\alpha_o = 0.018$ for the Argonaut reactor. Boynton (6) referred to reactivity measurements performed in the UFTR and reported an average value of the multiplication factor (of one core) of 0.81. This implies that a rough approximation of the reactivity coupling coefficient may be $\alpha_o = 0.19$. The basis of the comparison is the fact that the 18-inch core separation of the UTR-10 falls between the values of the core separation distances of Argonaut (24 inches) and UFTR (12 inches). Hence, the measured value of α_o for the UTR-10 may be expected to, and does, fall between $\alpha_o = 0.018$ and $\alpha_o = 0.19$.

VI. CONCLUSIONS

The mathematical model developed in this study shows that the real part of the cross-spectral density function of the fluctuating neutron density (at the detector locations) should vanish at a particular frequency, termed the sink frequency. This unusual behavior was discovered and verified in the experimental part of this investigation. The model adequately describes the shape of the measured magnitude of the cross-spectral density function in the neighborhood of the sink frequency.

Under the conditions of the proposed model, the sink frequency is related to the ratio of the reactivity coupling coefficient to the mean generation time in the cores and the times required for neutron disturbances to propagate between the cores and between the cores and the detector locations. Hence, with prior knowledge of the propagation times or, alternatively, with theoretically determined propagation times, the reactivity coupling coefficient of a coupled-core reactor may be estimated from the experimental measurement of the sink frequency.

Finally, it was demonstrated that an important coupled-reactor parameter can be evaluated by analyzing the noise information contained in the 10 to 200 cps frequency range wherein the effects of delayed neutrons can be completely ignored.

VII. SUGGESTIONS FOR FURTHER INVESTIGATION

The direct measurement of the times required for neutron disturbances to travel between regions in the reactor would provide a check on the validity of the neutron-wave model. This might be accomplished by determination of the phase lag between small amplitude variations of the neutron density at selected points in the cores and in the reflector.

A crosscorrelation analysis using digital techniques would, in theory, provide a more accurate measurement of the sink frequency. Access to an analog-to-digital conversion device would be required.

VIII. LITERATURE CITED

1. Badgley, R. W. and Uhrig, R. E. Power spectral density measurements in a subcritical nuclear reactor. Nuclear Science and Engineering 19: 158-163. 1964.

2. Balcomb, J. D., Demuth, H. B., and Gyftopoulos, E. P. A crosscorrelation method for measuring the impulse response of reactor systems. Nuclear Science and Engineering 11: 159-166. 1961.

3. Baldwin, G. C. Kinetics of a reactor composed of two loosely coupled cores. Nuclear Science and Engineering 6: 320-327. 1959.

4. Bendat, J. S. Principles and applications of random noise theory. New York, N.Y., John Wiley and Sons, Inc. 1958.

5. _____ and Piersol, A. G. Measurement and analysis of random data. New York, N.Y., John Wiley and Sons, Inc. 1966.

6. Boynton, A. R. Evaluation of parameters in a two slab reactor by random noise measurements. Unpublished Ph.D. thesis. Gainesville, Florida, Library, University of Florida. 1962.

7. _____ and Uhrig, R. E. Evaluation of two-region-reactor parameters by random noise measurements. Nuclear Science and Engineering 18: 220-229. 1964.

8. Cohn, C. E. Applicability of simple reactor kinetics to the interpretation of reactor noise experiments. In A Symposium on Noise Analysis in Nuclear Systems, Proceedings, University of Florida, 1963. pp. 307-320. Washington, D. C., Division of Technical Information, U. S. Atomic Energy Commission. 1964.

9. _____ Determination of reactor kinetic parameters by pile noise analysis. Nuclear Science and Engineering 5: 331-335. 1959.

10. _____ A simplified theory of pile noise. Nuclear Science and Engineering 7: 472-475. 1960.

11. Danofsky, R. A. Cross power spectral measurements in the University Training Reactor-10. In A Symposium on Noise Analysis in Nuclear Systems, Proceedings, University of Florida, 1963. pp. 229-250. Washington, D. C., Division of Technical Information, U. S. Atomic Energy Commission. 1964.

12. _____ and Uhrig, R. E. The kinetic behavior of the coupled regions of the UTR-10 reactor. Nuclear Science and Engineering 16: 131-133. 1963.

13. Griffen, C. W. and Randall, R. L. At power, low-frequency reactor-power-spectrum measurements and comparison with oscillation measurements. Nuclear Science and Engineering 15: 131-138. 1963.

14. Harrer, J. M., Boyer, R. E., and Krucoff, D. Transfer function of Argonne CP-2 reactor. Nucleonics 10, No. 8: 32-36. 1952.

15. Henry. A. F. and Curlee, N. J. Verification of a method for treating neutron space-time problems. Nuclear Science and Engineering 4: 727-744. 1958.

16. Kemeny, L. G. and Murgatroyd, W. Stochastic models for fission reactors. In A Symposium on Noise Analysis in Nuclear Systems, Proceedings, University of Florida, 1963. pp. 29-57. Washington, D. C., Division of Technical Information, U. S. Atomic Energy Commission. 1964.

17. Lee, Y. W. Statistical theory of communication. New York, N.Y., John Wiley and Sons, Inc. 1960.

18. Leribaux, H. R. Stochastic processes in coupled nuclear reactor cores. Unpublished Ph.D. thesis. Ames, Iowa, Library, Iowa State University of Science and Technology. 1963.

19. Moore, M. N. The determination of reactor transfer functions from measurements at steady operation. Nuclear Science and Engineering 3: 387-394. 1958.

20. _____ The power noise transfer function of a reactor. Nuclear Science and Engineering 6: 448-452. 1959.

21. Price, W. J. Nuclear radiation detection. 2nd ed. New York, N.Y., McGraw-Hill Book Co. 1964.

22. Rajagopal, V. Determination of reactor transfer functions by statistical correlation methods. Nuclear Science and Engineering 12: 218-224. 1962.

23. Sheff, J. R. and Albrecht, R. W. The space dependence of reactor noise. Nuclear Science and Engineering 24: 246-259. 1966.

24. Thie, J. A. Statistical analysis of power reactor noise. Nucleonics 17, No. 10: 102-111. 1959.

25. Weinberg, A. M. and Wigner, E. P. The physical theory of chain reactors. Chicago, Ill., The University of Chicago Press. 1958.

26. Wilson, E. B. An introduction to scientific research. New York, N.Y., Mc-Hill Book Co. 1952.

IX. ACKNOWLEDGMENTS

The author is indebted to his major professor, Dr. Glenn Murphy, Distinguished Professor and Head of the Department of Nuclear Engineering, for the support and guidance he provided throughout the investigation and preparation of the thesis.

The many helpful discussions with Dr. Richard Danofsky, Associate Professor of Nuclear Engineering, are gratefully acknowledged.

X. APPENDIX A

Derivation of Noise Source Spectra

The spectral densities of the fluctuating noise sources are evaluated by a method suggested by Cohn (10) and extended by Sheff and Albrecht (23) and Danofsky.[1] The internal noise sources each consist of three uncorrelated random processes: (1) fission absorption, (2) non-fission absorption, and (3) neutron exchange. Since it is assumed that the processes are uncorrelated, the Schottky formula is used to derive the spectra. The spectral density is given by

$$\Lambda = \sum_i q_i^2 \bar{m}_i \tag{77}$$

where Λ has units of n^2/cm^3 - sec, q_i is the net number of neutrons produced in a process of type i, and $\bar{m}_i$ is the average rate of occurence of the i^{th} process. The various source processes are listed in Table 1, where L is the generation time, including leakage, and g is the fraction of destructive processes which result in fission.

The spectral density of the noise source for core 1 is

$$\Lambda_{11} = \frac{n_{10}}{L}(1-g) + \frac{n_{10}}{L} g \sum_\nu (\nu - 1)^2 P(\nu) + \frac{\alpha_o}{L} n_{20} \tag{78}$$

---

[1] Danofsky, R. A. Ames, Iowa. Spectral density of noise sources. Private communication. 1966.

Table 1. Summary of noise source contributions in core 1.

Process	Average rate of occurrence	Net number of neutrons produced
non-fission absorption	$\frac{n_{10}}{L}(1 - g)$	-1
fission absorption	$\frac{n_{10}}{L} gP(\nu)$	$(\nu - 1)$
exchange	$\frac{\alpha_o}{L} n_{20}$	+1

where $P(\nu)$ is the probability that a fission will produce ν prompt neutrons. When the fundamental relationships,

$$\sum_{\nu} P(\nu) = 1$$

$$\sum_{\nu} \nu P(\nu) = \bar{\nu}$$

$$\sum_{\nu} \nu^2 P(\nu) = \overline{\nu^2}$$

are substituted into Equation 78, the result is

$$\Lambda_{11} = \frac{n_{10}}{L}\left[1 + g(\overline{\nu^2} - 2\bar{\nu})\right] + \frac{\alpha_o}{L} n_{20} . \qquad (79)$$

Similarily, the noise source for core 2 is

$$\Lambda_{22} = \frac{n_{20}}{L}\left[1 + g(\overline{\nu^2} - 2\bar{\nu})\right] + \frac{\alpha_o}{L} n_{10} \,. \qquad (80)$$

A relationship between g and the steady-state reactivity, δk, is developed by observing that the ratio of steady-state neutron production rate, P.R., to neutron destruction rate, D.R., is

$$\left[\frac{\text{P.R.}}{\text{D.R.}}\right]_{10} = g\bar{\nu} \,.$$

Now

$$\delta k_{10} = \left[\frac{\text{P.R.} - \text{D.R.}}{\text{P.R.}}\right]_{10} ,$$

so that,

$$\delta k_{10} = 1 - \frac{1}{g\bar{\nu}} \,.$$

Therefore, g in Equation 79 , for example, is replaced with

$$\frac{1}{(1 - \delta k_{10})\bar{\nu}}$$

But the steady-state conditions give

$$\delta k_{10} = -\alpha_o T \,,$$

and

$$\delta k_{20} = -\alpha_o / T \,.$$

Thus, Equations 79 and 80 become, respectively,

$$\Lambda_{11} = \frac{n_{10}}{L}\left[1 + \frac{1}{1 + \alpha_o T}\left(\frac{\overline{v^2} - 2\bar{v}}{\bar{v}}\right) + \alpha_o T\right] \tag{81}$$

and

$$\Lambda_{22} = \frac{n_{10}}{L}\left[1 + \frac{1}{1 + \alpha_o/T}\left(\frac{\overline{v^2} - 2\bar{v}}{\bar{v}}\right) + \alpha_o/T\right] . \tag{82}$$

XI. APPENDIX B

Analysis of Errors

Two types of errors associated with the analysis of random signals will be considered here. It will be shown that the bias portion of the statistical error dominates in the neighborhood of the sink frequency of the measured spectrum, and that the variance portion of the statistical error is greater in the low frequency region of the spectrum.

Within the category of statistical errors, the problem of bias must be recognized and analyzed when the magnitude of spectral data changes rapidly with frequency. Clearly, this is the case for the data in the vicinity of the sink frequency. A parameter estimate is said to be unbiased if the expected value of the estimate $\hat{C}_{xy}$ (obtained in the finite sampling time T) is equal to the true value of the parameter C_{xy}. In the expression for the normalized mean square error in spectral density measurements (5),

$$\varepsilon^2 = \frac{1}{B_e T} + \frac{B_e^4}{576} \left| \frac{C''_{xy}}{C_{xy}} \right|^2 , \tag{83}$$

(where B_e is the analyzer filter bandwidth, T is the sampling time, and C''_{xy} is the second derivative of the spectral density with respect to frequency), it is clear that the

error is reduced by increasing the bandwidth, provided the bias term is very small. Unfortunately, increased bandwidth decreases the resolution of the analyzer, and an increase in the bias term results when the contribution of C''_{xy} is significant. Bias errors are limited to about 3 percent in spectral density measurements of resonant systems if

$$B_e < \tfrac{1}{4} B_{sr} , \tag{84}$$

where B_{sr} is the bandwidth at the half-power point of the narrowest resonance measured (5). In terms of the above criterion, the bias contribution of Equation 83 becomes

$$\left[\frac{B_e}{\lambda(f)}\right]^4 = (576)(9 \times 10^{-4}) = 0.518 , \tag{85}$$

where $\lambda(f)$ is the spectral bandwidth,

$$\lambda(f) = \left|\frac{C_{xy}(f)}{C''_{xy}(f)}\right|^{1/2} .$$

Then $\frac{B_e}{\lambda(f)} = 0.84$ is the ratio of analyzer bandwidth to spectral bandwidth that corresponds to Equation 83. A value of $B_{sr} = \frac{70}{4}$ cps was obtained by inspection of Figure 7, and $B_e = 13.3$ cps at 100 cps. Thus,

$$\frac{B_e}{B_{sr}/4} \cong 3 ,$$

and the bias portion of the normalized standard error is

$$\varepsilon_b = \pm 0.26 \ .$$

The bias errors of the measurements below 60 cps were negligibly small.

An expression for the normalized standard error of the measured magnitude of the cross-spectral density

$$\varepsilon_F = \frac{\sigma}{F} = \left\{ \left(\frac{\hat{C}_V}{F} \right)^4 \left[(\varepsilon_v + \varepsilon_b)^2 + \varepsilon_{CI}^2 \right] + \left(\frac{\hat{Q}_V}{F} \right)^4 \left[(\varepsilon_v + \varepsilon_b)^2 + \varepsilon_{QI}^2 \right] \right\}^{1/2} , \qquad (86)$$

was developed from the compounding of errors formula (26), where

$$F = (\hat{C}_V^2 + \hat{Q}_V^2)^{1/2} ,$$

$$\varepsilon_v = \left(\frac{1}{B_e T} \right)^{1/2} ,$$

ε_b is the bias portion of the normalized standard error, ε_{CI} is the normalized error of the co-spectral measurement, and ε_{QI} is the normalized error of the quad-spectral measurement.

The data summarized in Table 2 were obtained from measurements performed at 10 cps and 100 cps.

Normalized standard errors obtained from calculations using Equation 86 are listed in Table 3.

Table 2. Summary of error analysis data.

Frequency (cps)	$\hat{C}_V$ (volts)	$\hat{Q}_V$ (volts)	F (volts)	B_e (cps)	T (sec.)
10	10.2 ± 0.01	0	10.2	1.3	300
100	0.20 ± 0.01	0.10 ± 0.01	0.224	13.3	300

Table 3. Summary of normalized standard errors.

Frequency (cps)	ε_v	ε_b	ε_{CI}	ε_{QI}	ε_F
10	± 0.05	~0	~0	~0	± 0.05
100	± 0.02	± 0.26	± 0.05	± 0.10	± 0.27

XII. APPENDIX C

Experimental Data

The experimental data obtained from measurements of the cross-spectral density over the frequency range of 10 to 200 cps are presented in Tables 4 and 5.

Table 4. Tabulation of experimental data of Run #1.[a]

Frequency (cps)	V_M (volts)	$10 \log_{10} \frac{V_M \times 10^2}{f}$ (db)	Circuit Correction[b] (db)	Gain Correction[c] (db)	Normalized[d] Magnitude (db)
10	10.20	26.1	0.6	2.5	0
12	9.36	24.9	1.0	2.5	-0.8
16	7.74	22.9	2.0	2.5	-1.8
20	6.12	20.9	2.6	2.5	-3.2
24	5.23	19.4	3.5	2.5	-3.8
28	4.41	18.0	3.8	2.5	-4.9
32	3.35	16.2	4.4	2.5	-5.6
40	1.09	10.4	5.4	5.0	-8.4
52	1.22	9.7	7.3	2.5	-9.7
60	0.99	8.2	8.3	2.5	-10.2
72	0.71	5.9	10.2	2.5	-10.6
80	0.34	2.3	11.4	2.5	-13.0
88	0.38	2.3	12.6	0	-14.3
100	0.22	-0.5	13.9	0	-15.8
120	0.07	-6.5	16.4	0	-19.3
160	0.16	-4.4	21.4	0	-12.2
180	0.20	-3.5	23.6	0	-9.1
200	0.22	-3.5	25.0	0	-7.7

[a]All integration times were 300 seconds.

[b]Correction for count-rate circuit frequency response.

[c]Operational amplifier gains were adjusted to provide distortion-free signals to the multipliers.

[d]Data were normalized to the 10 cps measurement.